Journal of Hydrology 653 (2025) 132792

Contents lists available at ScienceDirect

Journal of Hydrology

journal homepage: www.elsevier.com/locate/jhydrol

Research papers

Groundwater hydrogeochemical changes predating and following the November 9, 2022 M_w 5.5 Adriatic offshore earthquake (central Italy)

Lorenzo Chemeri [a,b,*], Marco Taussi [a], Davide Fronzi [c], Jacopo Cabassi [d,e], Stefano Mazzoli [f], Alberto Tazioli [c], Alberto Renzulli [a], Orlando Vaselli [b,d]

[a] Department of Pure and Applied Sciences, University of Urbino Carlo Bo, Via Ca' Le Suore 2/4 61029 Urbino, Italy
[b] Department of Earth Sciences, University of Florence, Via G. La Pira 4 50121 Florence, Italy
[c] Department of Science and Matter Engineering, Environment and Urban Planning (SIMAU), Marche Polytechnic University, Via Brecce Bianche 12 60131 Ancona, Italy
[d] Institute of Geosciences and Earth Resources (IGG), National Research Council of ItalyItaly (CNR), Via G. La Pira 4 50121 Florence, Italy
[e] Istituto Nazionale di Geofisica e Vulcanologia (INGV), Sezione di Roma1, Via di Vigna Murata 605 00143 Roma, Italy
[f] Geology Division, School of Science and Technologies, University of Camerino, Camerino, Italy

ARTICLE INFO

This manuscript was handled by Corrado Corradini, Editor-in-Chief, with the assistance of Carla Saltalippi, Associate Editor

Keywords:
Seismic tracers
Earthquakes
Hydrogeochemistry
Adriatic offshore
Precursory changes

ABSTRACT

We report the results from a pre- and post-seismic water monitoring carried out in the Mt. Conero area (central Italy) to evaluate the earthquake-related variations on the water hydrogeochemistry related to the November 9, 2022 Adriatic offshore seismic sequence. This latter was characterized by two main events of M_w 5.5 and 5.2. The monitoring network included two wells and one piezometer located at ~50 km from the earthquake epicentre. The wells did not show relevant changes. Contrarily, the piezometer showed an overwhelming variation in its composition and Total Dissolved Solids (TDS) since four months before the mainshock, shifting from a low-salinity (TDS < 1000 mg/L) calcium-bicarbonate facies to a high-salinity (TDS > 3500 mg/L) sodium-chloride composition. Then, composition and TDS were restored about a week after the events. These changes were accompanied by strong increases in trace elements concentrations (e.g., B, Mn), which returned to the pre-seismic values in the days following the mainshock. The strong hydrogeochemical variations recorded at the piezometer were likely related with two different seismically-induced processes linked to a mixing between shallow Ca-HCO_3 and deep Na-Cl waters, and the bedrock's fracture unclogging. These variations are, to the best of our knowledge, among the largest ever observed before a seismic event or, at least, ever reported in the literature. These results prove hydrogeochemical monitoring for seismic surveillance can be highly effective. Besides, our work represents a further step in the development of a methodology that could potentially track geochemical changes ahead of larger, potentially dangerous earthquakes.

1. Introduction

Several studies in the last decades highlighted that earthquakes of moderate to large magnitude (M_w > 4) are able to produce detectable changes in the geochemical composition of the waters circulating close to the epicentral area and/or in hydrogeological features of the aquifers involved (King, 1986; Thomas, 1988; Cicerone et al., 2009; Skelton et al., 2014, 2019, 2024; Manga et al., 2016; Barberio et al., 2017, 2020; Hosono et al., 2019, 2020; Chiodini et al., 2020; Fronzi et al., 2020a; Martinelli et al., 2020; Franchini et al., 2021; Wang and Manga, 2021; Cambi et al., 2022; Cinti et al., 2023). These variations, also called *seismic tracers* (Martinelli, 2020), may be of different nature and are generally observed from months to days prior to the seismic event, concurrently or immediately after the earthquake (Thomas, 1998; Cicerone et al., 2009; Martinelli, 2020). Notable changes were related to (a) discharge rates of springs and streams (e.g., Manga and Rowland, 2009; Wang and Manga, 2015; Fronzi et al., 2020b, Valigi et al., 2020; Mammoliti et al., 2022), (b) piezometric level in wells (e.g., Kitagawa et al., 2006; Sil and Freymueller, 2006; Barberio et al., 2020), (c) chemical and isotopic composition of waters and dissolved gases (e.g., Barberio et al., 2017; Hosono et al., 2019; 2020; Skelton et al., 2019; 2024; Hosono and Masaki, 2020; Chiodini et al., 2020; Fronzi et al., 2021; Gori and Barberio, 2022) and (d) groundwater physicochemical parameters (e.g., King et al., 1994; Reddy et al., 2017).

* Corresponding author at: Department of Pure and Applied Sciences, University of Urbino Carlo Bo, Via Ca' Le Suore 2/4, 61029 Urbino, Italy.
E-mail address: l.chemeri@campus.uniurb.it (L. Chemeri).

https://doi.org/10.1016/j.jhydrol.2025.132792
Received 24 October 2024; Received in revised form 7 January 2025; Accepted 22 January 2025
Available online 1 February 2025

These modifications are considered to be produced by the earthquake and its preparation process (i.e., the seismic cycle), since several chemical and physical processes may be triggered by (Doglioni et al., 2014; Martinelli and Tamburello, 2020; Wang and Manga, 2021): (i) physical mixing between two previously non-communicating aquifers due to changes in the hydraulic pressure (e.g., Thomas, 1988; Cicerone et al., 2009; Skelton et al., 2014, 2019, 2024), (ii) physical release due to pore collapse (e.g., Cicerone et al., 2009), (iii) chemical release due to pressure-sensitive solubility (e.g., Thomas, 1988; Cicerone et al., 2009) or (iv) chemical release following increased interactions with new active rock surfaces (e.g., Boschetti et al., 2019; Skelton et al., 2024). Precursory changes were detected worldwide in different geological and geodynamic settings characterized by intense seismic activity. However, since these changes are often transitory and strictly site-sensitive, the identification of possible and suitable seismic precursors represents one of the major challenges for geoscientists (Lee et al., 2017, 2021; Martinelli, 2020; Franchini et al., 2021; Cinti et al., 2023; Skelton et al., 2024). Therefore, to improve scientific knowledge on this topic, the development of multi-parametric water monitoring networks located in seismic-prone areas is a fundamental step towards a better understanding of the relationship between the seismic cycles and the seismic tracers (Lee et al., 2017; 2021; Franchini et al., 2021).

Italy experienced in its past and recent history an intense seismic activity, with some earthquakes having magnitudes > 7.0 (e.g., the 1693 Noto Valley Earthquake with an estimated magnitude between 7.5 and 7.7 M_w, and the 7.3 M_w Strait of Messina Earthquake in 1908 which

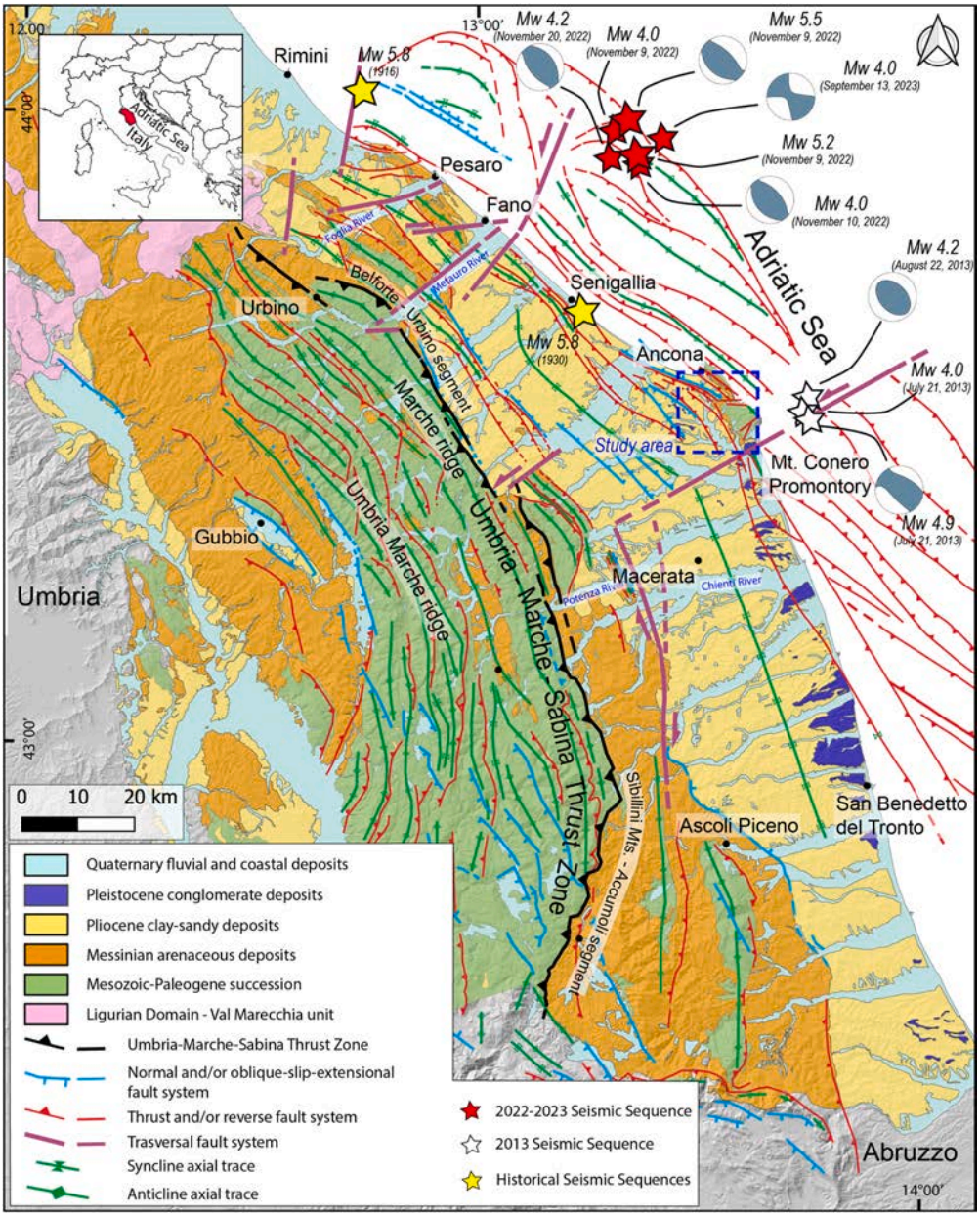

Fig. 1. Schematic geological map of the Marche Region and the offshore sector (modified from Teloni et al., 2024), showing the main tectonic structures and the location of the epicenters related to the offshore Adriatic Sea seismic sequence (November 2022), and the Mt. Conero seismic sequence (2013). Available focal mechanisms are also reported from terremoti.ingv.it. Location of the historical seismic sequences' main events are also represented (Rimini 1916: Bonini et al., 2016; Senigallia 1930: Vannoli et al., 2015).

caused about 80,000 fatalities). Most of the strongest earthquakes were associated with extensional faulting in the collapsing axial zone of the Apennines (Rovida et al., 2022). In the coastal area of central-eastern Italy and adjacent offshore, active thrust faults (DISS Working Group, 2021) caused the 1930 Senigallia earthquake (M_w 5.8; Vannoli et al., 2015) and the most recent offshore Adriatic Sea seismic sequence (maximum M_w 5.5) that occurred in front of the Marche Region coast on November 9, 2022 (Maesano et al., 2023; Pezzo et al., 2023). Water monitoring networks aimed at the identification of seismic precursors were deployed, focusing on both inland and coastal zones (Chemeri et al., 2024).

Here, we report the results obtained after the November 2022 seismic sequence from interseismic (i.e., a centennial time span dominated by long-term, steady behavior), pre-seismic and post-seismic (i.e., the relatively short time spans predating and postdating the seismic event(s) – in the order of months to several years – characterized by earthquake-related "perturbation" of hydrology or surface motion; Copley et al., 2012). The geochemical monitoring focused on groundwater collected from one piezometer, named Betelico (hereafter, BET), and two wells, named Vallemiano (hereafter, VAL) and Monte Acuto (hereafter, MAC), belonging to three distinct aquifers, with depths ranging from 15 (VAL and MAC) to 30 (BET) m and located to the west and northwest of the Mt. Conero Area (Marche Region) (Fig. 1). The aim of this work was to evaluate and assess possible earthquake-related variations of the water chemical and isotopic composition, highlighting the potential occurrence of precursory changes in the monitored sampling sites.

2. Geological and tectonic setting of the Mt. Conero area

The Mt. Conero is a coastal promontory located in the central-eastern sector of the Italian peninsula, south of Ancona (Marche Region, central-eastern Italy, Fig. 1). It shows a maximum altitude of 572 m a.s.l (Fig. 1) which breaks the continuity of the coastal shore along the Italian side of the Adriatic Sea. Almost the entire Conero area is classified as a public natural reserve and a popular touristic destination (Mussi et al., 2017; Mammoliti et al., 2023). Following the Köppen classification (Köppen and Geiger, 1954*)*, the climate of the area is "*temperate*" and "*sublittoral*" (i.e., *Cfa type*, humid subtropical climate) with an average rainfall of 900 mm/year, a monthly minimum precipitation in July (30 mm) and a maximum one in September (110 mm). The average atmospheric temperature varies from 14.1 °C to 16.6 °C in promontory and the coastal area, respectively (Mussi et al., 2017).

2.1. Tectonic framework and seismicity of the study area

The study area is located within the Umbria-Marche Apennines and foothills, which form part of the *peri*-Mediterranean Alpine orogenic belt (Figs. 1 and 2a). The Apennines are an arcuate, mostly NW-SE striking belt (Calamita et al., 1994). It evolved during the Neogene, in the frame of Africa-Eurasia plate convergence since the Late Cretaceous (Dewey et al., 1989; Mazzoli and Helman, 1994; Turco et al., 2021). Since the Late Miocene, back-arc extension in the hinterland (Tyrrhenian Sea) was coeval with thrusting in the frontal part of the belt (e.g., Butler et al., 2004). Therefore, the Apennines represent a mountain belt characterized by various, active geodynamic processes (Mantovani et al., 2014 and therein references). Extension and crustal thinning in the western side of the orogen are well established, as are tectonic accretion and crustal thickening in the eastern side.

The Umbria-Marche Apennines and foothills consist of a Meso-Cenozoic calcareous-marly succession that was progressively involved in the fold and thrust belt from west to east, as shown by synorogenic siliciclastic deposits filling a migrating foreland basin system. The basement was also involved in the thrust system (e.g., Coward et al., 1999). Transversal faults (probably inherited from the pre-orogenic stage) also controlled differential shortening in adjacent crustal sectors (Calamita et al., 1994; Calamita and Pizzi, 1994). A general eastward migration of the thrust front toward the foreland characterized the Pliocene to present time (Patacca et al., 1991; Barchi et al., 2012), while extension affected the hinterland and then the axial zone of the Umbria-Marche Apennines, generating NW-SE-striking crustal normal fault (Dewey, 1989; Keller et al., 1994; Doglioni, 1995; Barchi and Mirabella, 2009). Active thrusts in the Adriatic offshore are buried by thick Pliocene-Quaternary foreland basin deposits whose sedimentation rate largely exceeded those of thrust slip (e.g., Vannoli et al., 2004, 2015; Basili and Barba, 2007).

To date, the Mt. Conero area is characterized by moderate seismicity due to the presence of major composite seismogenic sources – able to produce earthquakes with a magnitude > 6 – running within or close to the study area (DISS Working Group, 2021). The active tectonics is generally associated with compressive and transpressive structures (Mazzoli et al., 2005, 2014, 2015; Chicco et al., 2019; Pierantoni et al., 2019; Maesano et al., 2023; Pezzo et al., 2023). The Adriatic coast, although affected by seismic events characterized by lower magnitudes and frequency compared to those occurring along the Apennine chain (Lavecchia et al., 1994, 2003; Mantovani et al., 2014; Rovida et al., 2022), experienced moderate seismicity throughout the last century, e.g., the 1916 Rimini seismic sequence with the mainshock characterized by a maximum magnitude of 5.8 (Fig. 1), the 1930 Senigallia earthquake (maximum M_w 5.8; Fig. 1), related to NW-SE striking thrusts (Vannoli et al., 2015; Bonini et al., 2016), and the 2013 Mt. Conero seismic sequence related to NE-SW striking strike-slip faults and NW-SE striking thrusts (maximum M_w 4.9; Mazzoli et al., 2014; Fig. 1). The most recent events (5.5 and 5.2 M_w) occurred on the morning of November 9, 2022. It consisted of a rapid sequence of earthquakes, a few minutes from each other, with epicenters located offshore the Adriatic Sea (Lat. 43.9830, Long. 13.4240), in front of the Marche Region and 50 km north of the city of Ancona (Figs. 1 and 2a). The seismic sequence also included three shocks with M_w between 4 and 5, and twenty-seven events with magnitude between 3 and 4 (Maesano et al., 2023; Pezzo et al., 2023). According to the first published studies, the November 2022 seismic sequence occurred along the most external structure in this sector of the northern Apennine (Maesano et al., 2023; Pezzo et al., 2023), with the thrust front buried under Early Pliocene-Quaternary deposits (Fantoni and Franciosi, 2010; Maesano et al., 2013). The preliminary findings indicated that the seismic sequence nucleated along the Apennines compressional front (offshore the northern Adriatic Sea), and it was likely caused by the (re)activation of buried thrusts. According to Pezzo et al. (2023), the slip occurred along a ca. 24° SSW-dipping thrust fault located in an intermediate position with respect to the deeper and shallow detachments involving the Mesozoic carbonate sequence, whilst Maesano et al. (2023) identified the source of the earthquakes in the activation of the Cornelia thrust system, buried under a thick cover (about 2000 m) of marine and continental Plio-Pleistocene deposits and possibly hosting ruptures capable of producing seismic events up to 6.5 M_w or larger due to its features and size, if reactivated together with adjacent thrusts. The hypocentral depths of the main events were estimated between 5 and 10 km (Pezzo et al., 2023; terremoti.ingv.it).

2.2. Stratigraphical and hydrological features

The Mt. Conero ridge is considered as a *minor ridge* in the Adriatic external structural domain of the Apennines (Calamita et al.,1991) and can be defined as a wide asymmetric brachyanticline with Adriatic vergence and NW-SE axial trend (Marchesini, 1946; Scisciani, 2009; Cello and Tondi, 2014; Sarti and Coltorti, 2014; Mattioli, 2014; Mussi et al., 2017). The anticline is characterized by gently dipping bedding (<25°) on the western limb, whilst the strata are almost vertical on the eastern limb (Fig. 2b; Mussi et al., 2017).

The lithologies exposed in the Mt. Conero area belong to the Umbria-Marche Meso-Cenozoic succession (Fig. 1 and 2a, b) (Nanni, 1980, 1991; Nanni et al., 1997; ISPRA, 2011). In this area, the Maiolica Fm (Upper

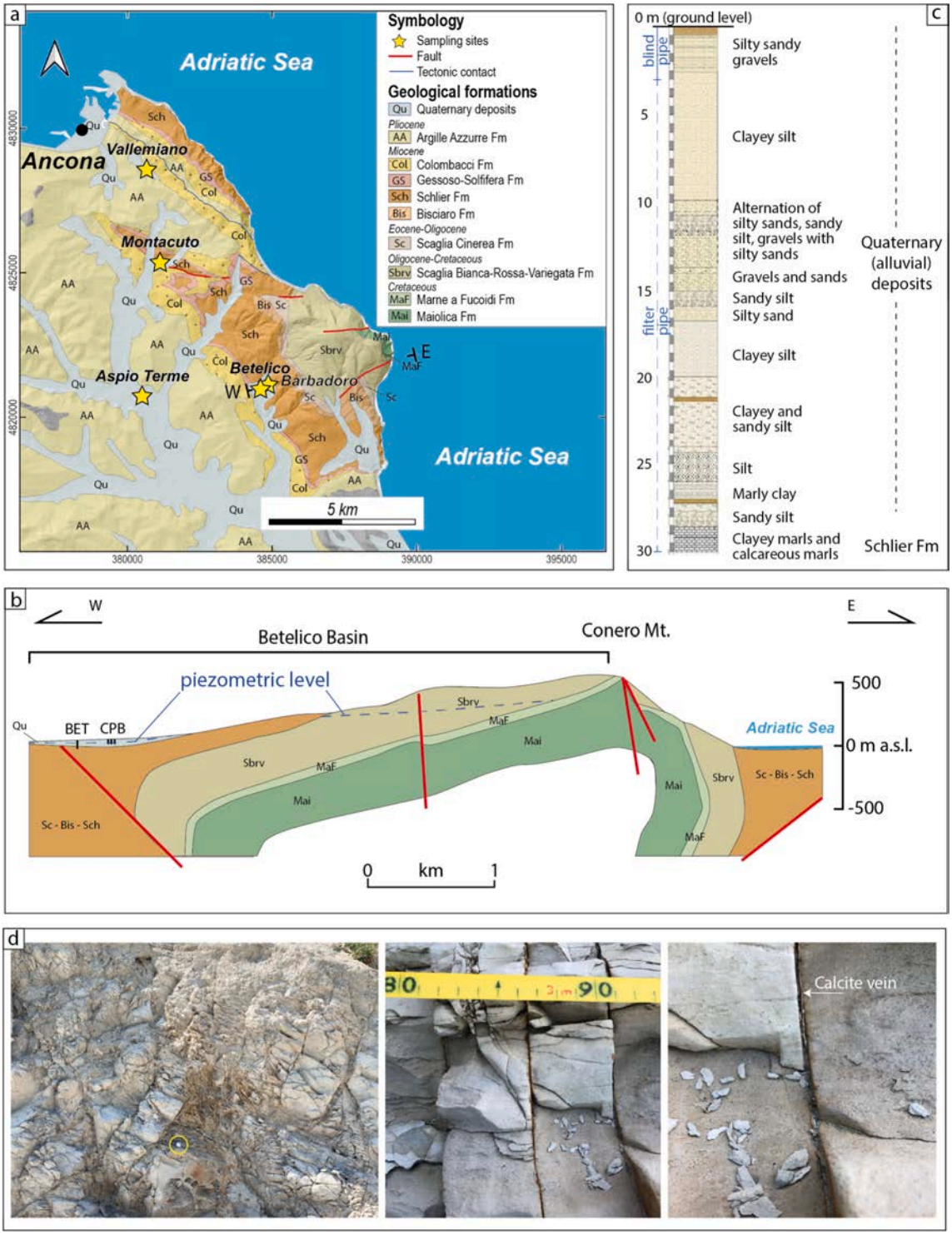

Fig. 2. (a) Geological map of the study area (modified from Conti et al., 2020) with the location of the sampling sites (Betelico, BET; Vallemiano, VAL; Monte Acuto, MAC; Barbadoro well field, CPB) and the Aspio Terme thermal springs; (b) stratigraphic details of the BET piezometer across the Quaternary alluvial deposits and the Schlier Fm with indicated the blind and fissured portion of the pipe; (c) schematic hydrogeologic cross-section of the BET area modified from Fronzi et al. (2022); (d) composite panel showing detail photographs of the extension fractures in marly limestone of the Schlier Fm from the outcrops in the surrounding of the study area. The composite filing includes both clay and vein calcite. Note that the calcite vein crosscuts the clay filling (arrow), as it is adjacent to the right wall in the upper part of the fracture and to the left wall in the lower sector. The occurrence of a *syn*-tectonic calcite vein cutting across the clay infill indicates that this latter, which predates the calcite vein formation, was produced by *syn*-tectonic clay injection within the fracture in subsurface conditions and does not represent a recent fracture infill at the surface. Therefore, the clay material consists of fine-grained sediments originally contained within the marine stratigraphic succession of the Schlier Fm.

Jurassic-Lower Cretaceous) represents the most ancient outcropping portion of the Umbria-Marche succession, and it mainly consists of micritic and compact limestones and calcarenites with thin shaly and bituminous interlayers (Mussi et al., 2017). Stratigraphically overlying the Maiolica Fm, the succession includes: (a) the Marne a Fucoidi Fm (Lower Cretaceous), outcropping on the coastal side of the ridge, made of silty shales and bituminous silty marls with chert nodules and lists; (b) the calcareous portion of the Scaglia Group (including the Scaglia Bianca, Scaglia Rossa and Scaglia Variegata Fms; Upper Cretaceous-Middle Eocene), mainly consisting of limestone, marly limestones and calcareous marls with an increase in the marly components in the upper portions; (c) the Scaglia Cinerea Fm (Upper Eocene-Upper Oligocene), which is mainly characterized by calcareous marls and shaly marls, followed by marls and marly shales (ISPRA, 2011; Mussi et al., 2017). The Miocene part of the succession starts with the Bisciaro Fm (Lower Miocene), which consists of marly and siliceous marly limestones. It is followed by the Schlier Fm (Lower Miocene-Upper Miocene) that is dominated by shaly marls, calcareous marls and shales. The Schlier Fm in the Mt. Conero area reaches the Messinian (ISPRA, 2011) and is overlain by the Gessoso-Solfifera Fm, here represented by the Sapigno Fm. This is formed by an alternation of mainly bituminous shales, gypsum-arenites, crystalline gypsum, diatomites and sulfur-rich limestones (ISPRA, 2011). The upper most Miocene (Messinian) unit is represented by the Colombacci Fm, which includes shaly marls and shales with arenaceous intercalations. The Lower Pliocene Argille Azzurre Fm overlies an unconformity exposed right to the west of the Betelico Creek. These Lower Pliocene deposits include shales and interbedded sandstones. The unconformably overlying Pleistocene to Holocene continental deposits are generally represented by alluvial (or debris) deposits composed of alternating calcareous gravels, clays, silty-clays, and sand (ISPRA, 2011; Mussi et al., 2017), as those penetrated by the BET borehole.

Concerning the hydrogeology of the Mt. Conero territory, the area is drained by some perennial and seasonal streams, of which the Betelico and Boranico creeks are the most important, being both tributaries of the Aspio River at south-west (Tazioli et al., 2015; Busico et al., 2020, 2024). Moreover, three main aquifers can be identified: the first one hosted in the carbonate deposits of the Scaglia Fms, and the others, both shallow, located in the alluvial deposits of the Betelico creek and in the stratified debris slope deposits (Mussi et al., 2017; Fronzi et al., 2021b, 2024), respectively. The Scaglia aquifer is the most important source for the water supply of the area, being confined by two impervious marly-shaly formations, i.e., the Marne a Fucoidi Fm at the bottom and the Scaglia Cinerea at the top. Additionally, the Scaglia aquifer is laterally sealed by the marly aquicludes hence hydraulically separated from the shallow aquifers (Mussi et al., 2017). Furthermore, the occurrence of highly saline connate waters trapped within the foredeep clayey sediments or at the bottom of alluvial aquifers is widely reported in the literature (e.g., Nanni and Vivalda, 1999, 2005). Such waters generally show a Na-Cl composition and TDS values almost comparable to those of seawater. Additionally, the occurrence of high salinity springs, whose pathways toward the surface are favored by the presence of local structures (e.g., the Boranico Springs), in the Mt. Conero area are also reported (Mattioli, 2014).

3. Materials and methods

The BET standpipe piezometer and the VAL and MAC wells, located ca. 45–55 km from the epicenter (Fig. 1) of the November 9, 2022 earthquakes, were selected in the Mt. Conero area for a seismic water monitoring of the offshore seismic events (Table 1). The selected points (Table 1) are all hosted in Quaternary alluvial deposits and pertain to three different alluvial aquifers (Fig. 2a). VAL and MAC are masonry wells with a diameter of ~ 1 m and a maximum depth of 15 m below ground level (b.g.l.). On the other hand, BET consists of a borehole lined with PVC filter pipe of 4′′ diameter from 3 to 30 m depth b.g.l., while the remaining top section (from 0 to 3 m b.g.l.) is lined with a PVC blind pipe (Fig. 2c). The pipe allows groundwater to rise inside, indicating the pore water pressure or hydraulic head in the investigated groundwater body at a specific point and specific time, and offers the opportunity to sample groundwater.

Table 1
Geographic location (WGS84), depth and distance from the epicenter of the seismic event of wells and piezometer.

Site	Latitude	Longitude	Depth (m)	Distance (km)
BET	43.533085	13.571422	30	55
CPB	43.534743	13.573257	9	55
VAL	43.600672	13.521379	15	45
MAC	43.571916	13.527878	15	50

All waters were sampled within 48 h (Nov 11, 2022), one week (Nov 17, 2022) and one month (Dec 12, 2022) after the mainshock and then, periodically for one year after the event. Specifically, BET was sampled 8 times on a monthly/bimonthly basis (Jan 17, Feb 14, Mar 15, Apr 17, May 18, Jul 19, Sep 29 and Nov 6, 2023), whereas MAC and VAL were sampled three times on a quarterly basis (Feb 14, Jul 19 and Nov 6, 2023). MAC was not sampled in July 2023 since it was temporarily inaccessible. Moreover, BET was sampled from May to Oct 2022, specifically on May 5, Jun 30, Sep 9, Sep 30, and Oct 25, 2022 (5 samples). The sampling operations were conducted using a bailer sampler within the uppermost 2 m of the saturated zone of the investigated aquifers. Previous (from 2006 to 2023) water chemical analysis from the "Barbadoro" wells field (CPB), made up of four wells (i.e., CPBw1 to CPBw4) 9 m depth b.g.l. and lined with 0.4 m diameter steel filter pipes, located ca. 200 m east and at a slightly higher altitude from BET and pumping from the same aquifer were also available (Fig. 2a). Specifically, the chemical analysis from 2006 to 2012 are referred to the loading tank (CPBwt) where the waters from CPBw1, CPBw2 and CPBw3 converged, whilst from 2013 to 2023, water chemistry for each well is available.

Starting from January 2016, BET was equipped with a hydrometric pressure transducer (TD-Diver Eijkelkamp, accuracy ± 0.5 cmH_2O and resolution 0.2 cmH_2O) compensated by atmospheric pressure, for continuously monitoring groundwater level fluctuation and temperature at daily scale. Precipitation (P) and air temperature (T_{air}) in the area were monitored through a thermo-pluviometric station (Fronzi et al., 2024). Starting from January 2022, the vadose zone of the CPB area was supplied with three TDR sensors TEROS 12 (Meter Group Inc., Pullman, WA, USA) placed into the soil deposits of the alluvial aquifer at 0.6, 0.9, and 1.7 m depth. The TDR sensors record the volumetric water content (VWC), soil temperature (T_{soil}) and bulk electric conductivity (bEC) every fifteen minutes, allowing to characterize the aquifer recharge under the effect of different precipitation events and exclude any groundwater hydrochemical modification due to the recharge of meteoric waters. Technical specifications about the resolution and accuracy for the TDR sensors are reported in Fronzi et al. (2024).

In 2017, 2023 and 2024, four vertical logs were carried out at BET and performed by using a CTD-Diver Eijkelkam (accuracy ± 5 cmH_2O, ± 1 % of Electric Conductivity measure, and resolution 2 cmH_2O, 0.1 % of Electric Conductivity measure) compensated by atmospheric pressure to observe any groundwater body stratification in terms of electrical conductivity (EC).

Water temperature (in °C, resolution 0.1 °C, accuracy ± 0.1 °C), EC (compensated at 25 °C; resolution 0.1 % of reading mS/cm, accuracy ± 1 % of reading mS/cm), and pH (resolution 0.1 pH; accuracy ± 0.1 pH) were determined in situ during the sampling phases using an *AQUA-READ AP-800* (Aquaread Ltd. Broadstairs, UK) whilst the water table depth was measured with a phreatimeter (in m b.g.l.). Water aliquots were collected as follows: (a) unfiltered aliquot in 125 mL polyethylene (PE) bottle for the analysis of the main anions (HCO_3^-, F^-, Cl^-, Br^-, NO_3^-, SO_4^{2-}), SiO_2, B and NH_4^+; (b) filtered (0.45 μm) and acidified (with 1 % Suprapur HCl) aliquot in 50 mL PE bottle for the analysis of the main

cations (Ca^{2+}, Mg^{2+}, Na^{+}, K^{+}); (c) filtered (0.45 μm) and acidified (with 1 % Suprapur HNO_3) aliquot in 50 mL PE bottle for trace elements (Li, V, Co, Mn, Fe, Cr, Cu, Ni, Zn, As, Rb, Sr, Ba, Pb) and (d) unfiltered aliquot in 15 mL PE tube for the analysis of the water stable isotopes (δ^2H and $\delta^{18}O$).

Alkalinity (as HCO_3^-) was determined through acidimetric titration (AT) with HCl (0.01 M) and methyl-orange as colorimetric indicator, ammonium (NH_4^+) was analyzed with the Nessler Method via molecular spectrophotometry (MSP) with a HACH DR2100 instrument whilst the concentrations of major anions (F^-, Cl^-, Br^-, NO_3^- and SO_4^{2-}) and cations (Na^+, K^+, Mg^{2+} and Ca^{2+}) were determined by ion chromatography, using a Metrohm 761 Advanced Compact IC and a Metrohm 861 Compact IC, respectively. The analytical error for AT, MSP and IC was < 5 % (Chemeri et al., 2024). Trace element concentrations were determined using Inductively Coupled Plasma – Mass Spectrometry (ICP-MS) with an Agilent 7800 mass spectrometer, equipped with a quadrupole. The analytical error was < 10 % (Cinti et al., 2023). The determination of hydrogen ($^2H/^1H$ and expressed as δ^2H‰ vs. V-SMOW) and oxygen ($^{18}O/^{16}O$ and expressed as $\delta^{18}O$‰ vs. V-SMOW) isotopic ratios of the water molecule were performed via wavelength-scanned cavity-ring down spectroscopy (WS-CRDS) using a near-infrared laser analyzer (Picarro L2130-i), with analytical errors: $\delta^2H \pm 0.5$ ‰, $\delta^{18}O \pm 0.08$ ‰ vs. V-SMOW. All the chemical and isotopic analyses were carried out at the Laboratory of Fluid Geochemistry of the Department of Earth Sciences, University of Florence except for SiO_2 and B contents that were performed at the laboratories of Gruppo C.S.A. S.p.A (Rimini, Italy), through ICP-AES and ICP-MS, respectively.

4. Results

4.1. Water chemistry

The complete results including pH, T (°C), water level depth (m b.g.l.), major anions and cations, and water stables isotopes are reported in Table 2, whilst trace element concentrations are listed in Table 3.

4.1.1. VAL and MAC wells

The pH values at MAC varied from 7.07 (Nov 17, 2022) and 7.53 (Feb 14, 2023), whilst at VAL they ranged between 7.43 (Jul 19, 2023) and 7.90 (Feb 14, 2023). Water temperature was between 11.6 (Dec 12, 2022) and 17.2 °C (Nov 11, 2022) and between 9.6 (Feb 14, 2023) and 16.2 °C (Jul 19, 2023), at MAC and VAL sites, respectively. At MAC, the water level varied from 1.35 m below the surface, in Feb 2023, to 3.10 m, in Nov 11, 2022, whereas at VAL, it was varying between 1.94 m, (Feb 2023), and 5.29 m (Nov 2023). None of these parameters showed significant variations in the period following the seismic events.

The TDS values at MAC ranged between 855 and 894 mg/L (Fig. 3a) and from 739 to 932 mg/L at VAL (Fig. 3b). Among major anions, both sites were dominated by HCO_3^-, ranging between 445 and 461 mg/L at MAC, and 424 and 573 mg/L at VAL. Sulfate contents at MAC were higher than those of VAL being comprised between 94 and 104 mg/L, and 51 and 65 mg/L, respectively, whilst Cl^- ranged from 45 to 53 mg/L at MAC, and from 62 to 79 mg/L at VAL. Both sites were characterized by relatively low contents of F^- (<0.6 mg/L) and Br^- (<0.5 mg/L). VAL also showed low NO_3^- concentrations (<5 mg/L) while at MAC nitrate ranged from 30 to 58 mg/L. Concerning cations, Ca^{2+} was dominant in both sites (from 169 to 185 mg/L, and from 100 to 138 mg/L at MAC and VAL, respectively), Na^+ was present in higher contents at VAL, varying from 53 to 74 mg/L, whilst it was ranging between 37 and 41 mg/L at MAC. VAL had Mg^{2+} contents between 26 and 38 mg/L while those of MAC were from 20 to 21 mg/L. Both sites showed low contents of K^+ (<4 mg/L). Eventually, the NH_4^+ content was always below 0.10 mg/L at MAC, while that of VAL was spanning in a larger range, from 0.01 up to 2.0 mg/L. Both MAC and VAL had a constant Ca-HCO_3 composition for the entire monitoring period with no notable changes in the days following the seismic events and during the following year (Fig. 3a, b).

Similarly, the concentrations of trace elements did not show relevant variation at both sites during the monitoring period with just a few exceptions (Table 3; Fig. 3c, d). At VAL, Fe, Cu and Zn displayed their maximum contents of 195 μg/L, 31 μg/L and 32 μg/L, respectively, on Nov 11, 2022 (i.e., two days after the main earthquakes) and their contents slowly decreased in the following surveys. Copper and Zn showed a similar behavior at the MAC with the highest concentrations

Table 2
Water physicochemical parameters (pH, T in °C). Major anions (HCO_3^-, F^-, Cl^-, Br^-, NO_3^- and SO_4^{2-}), cations (Ca^{2+}, Mg^{2+}, Na^+, K^+), and Total Dissolved Solids (TDS) are reported in mg/L. Water level (wl) reported in m b.g.l. Water stable isotopes are expressed as ‰ V-SMOW. (n.d. = not determined; bdl = below detection limit).

Site	Date	pH	T	wl	HCO_3	F	Cl	Br	NO_3	SO_4	Ca	Mg	Na	K	NH_4	TDS	$\delta^{18}O$	δ^2H
BET	05/05/22	6.50	n.d.	6.42	207	0.3	36	0.12	88.1	36	93	12	30	1.1	bdl	504	−7.87	−48.2
	30/06/22	n.d.	n.d.	9.19	381	2.0	2020	9.11	32.5	69	196	54	1189	1.7	0.07	3965	−8.10	−48.6
	09/09/22	6.85	n.d.	9.28	485	0.6	1977	7.87	35.7	66	216	59	1185	9.6	0.72	4038	−8.19	−48.2
	30/09/22	6.80	n.d.	9.09	479	0.8	1744	7.37	30.6	69	206	52	1101	5.6	0.07	3695	−8.22	−48.0
	25/10/22	6.83	n.d.	9.32	515	1.1	1916	7.82	31.5	64	223	51	1241	4.7	0.33	4058	−8.05	−47.6
	11/11/22	7.79	15.8	9.41	500	1.0	1566	6.46	2.6	41	158	42	991	6.1	5.40	3316	−8.06	−48.7
	17/11/22	7.24	13.3	9.13	366	0.7	164	0.59	11.6	41	101	12	127	2.9	0.09	827	−8.5	−49.3
	12/12/22	7.15	15.9	6.13	317	1.3	52	0.14	18.3	44	107	9	38	2.6	0.20	594	−8.55	−48.3
	17/01/23	7.12	15.4	4.35	317	0.5	53	0.15	35.5	44	126	10	37	6.9	bdl	627	−7.99	−45.8
	14/02/23	7.69	15.3	2.12	356	0.4	45	0.27	40.5	39	130	11	34	4.0	0.03	657	−8.18	−48.2
	15/03/23	7.02	n.d.	2.61	348	0.3	32	0.19	75.5	33	125	10	30	1.0	0.05	655	−8.45	−48.0
	17/04/23	7.27	13.7	2.11	338	0.3	40	0.18	76.0	31	115	11	29	0.8	0.09	641	−8.20	−47.3
	18/05/23	7.34	14.0	1.77	350	0.5	54	0.16	49.6	36	129	11	27	1.0	0.03	658	−8.01	−46.6
	19/07/23	7.37	16.2	4.41	345	0.5	39	0.15	73.8	29	136	10	25	1.7	0.10	663	−7.92	−47.5
	29/09/23	7.52	16.5	6.54	342	0.7	57	0.12	34.8	34	130	10	29.	4.0	0.01	639	−8.37	−48.8
	11/11/23	7.34	15.6	7.38	421	0.7	72	0.21	30.7	38	159	13	35	1.6	0.08	773	−7.61	−45.2
VAL	11/11/22	7.81	15.3	5.23	570	0.5	63	0.27	0.2	53	131	33	74	3.9	1.98	932	−7.26	−41.5
	17/11/22	7.79	13.1	5.20	567	0.5	63	0.27	0.3	53	129	38	72	3.0	1.79	929	−7.37	−42.0
	12/12/22	7.56	11.1	5.12	573	0.5	65	0.28	3.5	55	123	36	70	3.1	1.85	932	−6.87	−40.2
	14/02/23	7.90	9.6	1.94	432	0.5	67	0.27	3.5	51	100	26	55	3.8	0.07	739	−13.2	−67.8
	19/07/23	7.43	16.2	4.02	424	0.9	62	0.24	2.0	53	114	28	53	2.3	0.13	739	−7.20	−39.3
	06/11/23	7.63	13.9	5.29	527	0.5	79	0.34	2.5	65	138	34	70	2.1	0.01	917	−6.97	−39.5
MAC	11/11/22	7.52	17.2	3.10	448	0.6	48	0.24	29.6	95	170	21	41	2.3	0.04	855	−8.26	−49.0
	17/11/22	7.07	11.8	3.03	451	0.5	47	0.22	30.5	97	169	21	41	2.2	0.01	859	−8.42	−48.3
	12/12/22	7.19	11.6	2.60	461	0.4	48	0.20	33.7	100	171	21	39	1.0	0.01	875	−7.92	−44.8
	14/02/23	7.53	12.8	1.35	448	0.6	45	0.33	37.3	104	170	20	38	1.0	0.07	864	−6.53	−40.5
	06/11/23	7.49	15.2	2.83	445	0.5	53	0.25	58.4	94	185	21	37	1.0	0.01	894	−7.25	−42.8

Table 3
Trace element concentrations. Si expressed as SiO_2 and reported in mg/L. B, Li, V, Cr, Mn, Fe, Co, Ni, Cu, Zn, As, Rb Sr, Ba and Pb reported in μg/L. (bdl = below detection limit).

Site	Date	SIO_2	B	LI	V	Cr	Mn	Fe	Co	Ni	Cu	Zn	As	Rb	Sr	Ba	Pb
BET	05/05/22	n.d.	n.d.	7.8	2.2	8.5	0.7	1.8	0.04	2.7	2.8	5.1	0.78	0.6	880	413	0.06
	30/06/22	36	4410	323	0.3	1.2	76	23	0.52	6.1	6.8	38.5	1.84	11.2	10,633	7266	0.82
	09/09/22	34	2940	302	0.2	1.1	4.2	9.7	0.12	7.1	14.4	22.3	1.04	11.2	9980	7268	0.50
	30/09/22	33	2820	286	0.2	1.0	1.5	7.6	0.06	4.8	11.4	16.1	1.04	10.2	9576	6762	0.98
	25/10/22	36	3200	347	0.2	1.0	108	31	0.18	4.7	3.7	19.1	0.86	10.4	11,184	7895	0.52
	11/11/22	33	2255	254	0.8	14.8	515	294	1.58	33.6	255	252	0.96	11.4	8354	5958	4.20
	17/11/22	21	369	284	0.8	14.7	518	290	1.34	12.5	100	108	0.69	9.7	8688	6231	1.02
	12/12/22	22	180	11.7	2.0	3.1	2.9	3.8	0.04	1.0	1.6	16.1	0.68	1.2	714	375	0.20
	17/01/23	24	154	8.5	1.9	3.9	19.5	42.0	0.28	2.4	3.8	19.4	0.78	1.5	648	316	1.39
	14/02/23	26	97	9.8	2.3	10.5	1.1	4.8	0.04	0.9	0.5	15.6	0.92	0.1	910	433	0.07
	15/03/23	23	67	10.4	2.1	9.5	0.7	3.5	0.03	0.8	1.1	5.6	0.70	0.2	1250	446	0.15
	17/04/23	23	57	9.6	2.0	6.3	6.1	117	0.13	1.6	2.2	22.7	0.70	0.5	921	439	2.30
	18/05/23	23	49	10.2	2.1	4.4	4.1	92	0.10	1.8	3.1	15.3	0.74	0.9	1162	475	1.05
	19/07/23	22	52	9.8	1.7	3.2	6.9	4.0	0.09	2.2	2.7	14.6	0.93	3.7	976	426	0.44
	29/09/23	23	104	10.5	2.2	5.7	1.5	13	bdl	1.5	4.5	7.2	0.81	0.5	965	410	0.22
	11/11/23	24	60	10.9	4.4	10.1	61	127	1.26	7.5	8.9	32.1	1.64	2.8	862	666	3.33
VAL	11/11/22	16	129	12.1	1.3	5.3	352	195	0.24	3.6	30.8	32.3	0.67	9.9	804	75	0.50
	17/11/22	15	132	12.1	0.9	0.1	346	147	0.11	0.7	1.3	2.2	0.50	8.8	798	70	0.02
	12/12/22	17	149	12.0	0.8	2.3	311	130	0.22	2.2	1.7	16.9	0.85	9.8	785	58	0.42
	14/02/23	13	104	9.6	3.8	1.0	8.8	19.2	0.07	1.3	3.9	6.5	0.84	5.3	514	39	0.13
	19/07/23	<1	93	11.5	2.6	0.2	271	5.8	0.16	4.9	1.9	2.9	0.55	4.5	515	45	0.03
	06/11/23	13	123	12.0	1.6	0.3	307	6.7	0.15	2.1	1.1	7.7	0.54	6.4	651	55	0.18
MAC	11/11/22	19	103	9.5	0.7	8.4	21	52	0.15	6.0	35.1	30.4	0.33	1.2	743	140	0.27
	17/11/22	18	87	9.4	0.8	7.7	18	51	0.14	4.6	4.2	17.0	0.35	1.2	728	104	0.35
	12/12/22	19	94	5.5	0.6	2.0	4	30	0.06	2.0	2.2	10.0	0.18	1.2	502	73	0.57
	14/02/23	20	83	8.9	0.6	1.8	2	4	0.05	1.7	0.6	4.7	0.20	0.3	734	103	0.11
	06/11/23	18	81	9.3	0.6	3.2	6	22	0.07	3.1	2.2	9.4	0.21	0.7	734	107	0.26

being detected on Nov 11, 2022 (35 μg/L, and 30 μg/L, respectively) and then decreased during the monitoring period.

The δ^2H values ranged from −49.0 ‰ to −40.5 ‰ V-SMOW at MAC site and from −67.8 ‰ to −39.3 ‰ V-SMOW at VAL whereas $\delta^{18}O$ values varied from −8.42 ‰ to −6.53 ‰, and from −13.20 ‰ to −6.87 ‰ V-SMOW at MAC and VAL, respectively.

4.1.2. The BET waters

At BET, the pH ranged from 6.50 to 7.79 (average 7.21), with the lowest value measured on May 5, 2022 and the highest value detected on Nov 11, 2022, i.e., two days after the event. Water temperature varied from 13.3 (Nov 17, 2022) to 16.5 °C (Sep 29, 2023) while the saturation depth ranged from 1.77 (May 18, 2023) to 9.41 (Nov 11, 2022) m b.g.l. Unfortunately, none of these data are available for the CPB wells.

The chemical composition at BET showed strong and striking variations between the pre- and post-seismic monitoring period (Fig. 4a). The TDS values increased from 504 mg/L (May 5, 2022) to 3965 mg/L (Jun 30, 2022) and maintained similar values until the mainshock (Table 2). Subsequently, the TDS content slightly decreased on Nov 11, 2022, two days after the seismic sequence (TDS = 3316 mg/L), and returned to pre-seismic values about a month after the event, i.e., from 827 mg/L (Nov 17, 2022) to 594 mg/L (Dec 12, 2022).

The TDS retained a content < 800 mg/L for an entire year after the main events (Dec 2022 – Nov 2023; Table 2).

The overwhelming changes measured for the TDS values were coupled with variations in terms of major components contents and geochemical facies (Fig. 4a). In fact, on May 5, 2022, BET showed a Ca-HCO_3 composition with low contents of Cl^- (36 mg/L) and Na^+ (30 mg/L), whilst on Jun 30, 2022, it displayed a Na-Cl geochemical facies that retained until Nov 11, 2022. Specifically, Cl^- contents increased more than fifty times (up to 2000 mg/L) and those of Na^+ increased almost forty times (up to 1200 mg/L) (Table 2). Moreover, setting aside Cl^- and Na^+, other elements showed slight to major changes: HCO_3^- increased from 207 to 515 mg/L, Br^- from 0.1 to 9.1 mg/L, SO_4^{2-} doubled its concentration (from 36 to 70 mg/L), Ca^{2+} increased from 93 to 223 mg/L, Mg^{2+} from 12 to 59 mg/L and K^+ from 2 to 9 mg/L. Contrarily, NO_3^- contents decreased from 88 to about 30 mg/L with the lowest concentration measured on Nov 11, 2022 (2.5 mg/L), whilst NH_4^+ did not show significant changes with the exception of the content detected on Nov 11, 2022 (5.40 mg/L), which was more than five times higher than those previously measured. All the ionic concentrations dropped to the contents similar to those measured on May 5, 2022 in less than a month (Dec 12, 2022) from the mainshock. The following surveys were characterized by concentrations that were approaching those related to the pre-event monitoring. In detail, over the Dec 2022–Nov 2023 monitoring period, Cl^- varied from 32 to 72 mg/L, Na^+ and Mg^{2+} were always below 40 mg/L and 15 mg/L, respectively, with Ca^{2+} and HCO_3^- as major components (Table 2; Fig. 4a).

The groundwater geochemical variability recorded at BET was not only limited to major elements. Slight to strong variations were indeed also observed for trace elements (Table 3; Fig. 4b, c, d). Specifically, following their behavior, the latter can be grouped in trace elements that (i) increased their contents from Jun 30, 2022 (i.e., *pre-seismic period*) together with the TDS and compositional changes (i.e., B, SiO_2, Ba, Sr, Li) (Fig. 4b), and (ii) showed their peak values (Mn, Fe, Cu, Zn, V, Cr, Co, Ni, Pb) following the November 9 seismic sequence, on Nov 11 and Nov 17, 2022 (Fig. 4c, d).

Boron content was between 2820 and 4410 μg/L during the period Jun-Oct 2022 then decreased to 2255 μg/L on Nov 11, 2022 and its content kept decreasing in Dec 2022 and Jan 2023 to 150 μg/L and retained lower values for the remaining monitoring period. Silica showed an average content of 34 mg/L during the pre- (Jun to Sep 2022) and inter-seismic (Oct and Nov 2022) time frame and after the event its concentrations remained around 24 mg/L. Lithium, Ba and Sr increased from Jun 30, 2022 up to 323 μg/L, 7895 μg/L and 11200 μg/L, respectively, and showed higher contents until Nov 17, 2022. An abrupt decrease was then observed and the concentrations were comparable to those measured on May 5, 2022, e.g., Li approximately 10 μg/L, Ba around 400 μg/L and Sr between 648 and 1250 μg/L (Fig. 4b).

Concerning transition metals, Mn had its peak values on Nov 11 (515 μg/L) and Nov 17 (518 μg/L) whilst during the other surveys its content was generally below 10 μg/L, with a few exceptions (Table 3), thus increasing almost fifty times in the days following the seismic event with

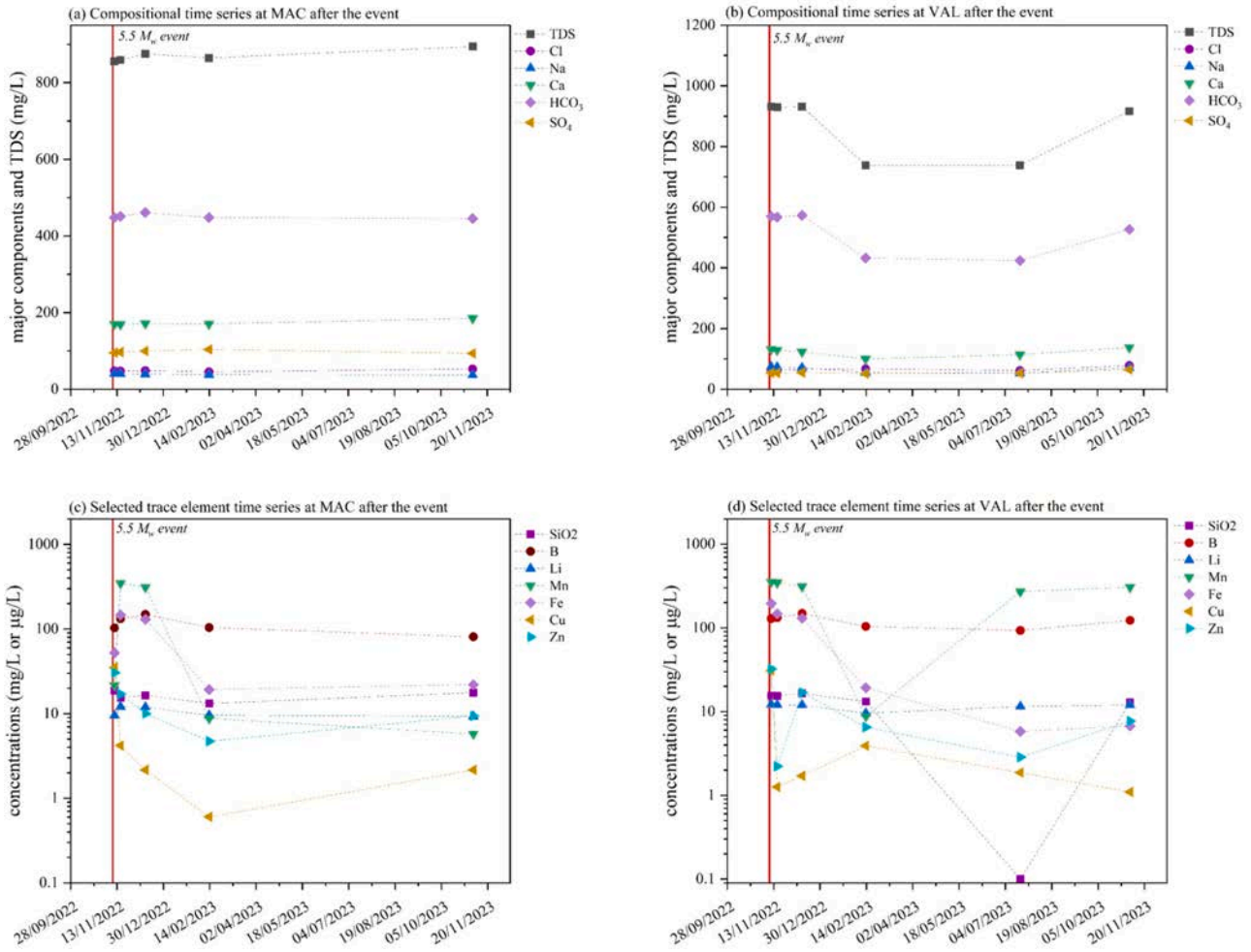

Fig. 3. Compositional variations at MAC and VAL sites over the November 2022 – November 2023 monitoring period: (a) major components and TDS (mg/L) and groundwater level at MAC; (b) major components and TDS (mg/L) at VAL; (c) selected trace elements (SiO_2, B, Li, Mn, Fe, Cu, Zn) at MAC; (d) selected trace elements at VAL. Trace element concentrations are reported in µg/L except for SiO_2 in mg/L. Vertical red line indicates the day of the seismic event (November 9, 2022; M_w = 5.5). (For interpretation of the references to color in this figure legend, the reader is referred to the web version of this article.)

respect to its average contents. Similarly, Cu reached the contents of 255 and 100 µg/L on Nov 11 and 17, respectively, whereas before and after the earthquake its concentrations rarely exceeded 10 µg/L. Zinc content was 252 µg/L (Nov 11) and 108 µg/L (Nov 17), displaying concentrations almost fourteen and six times, respectively, higher than its average content (< 20 µg/L) (Fig. 4c). Similar changes, though less relevant, were also detected for Fe (i.e., peak values of 294 and 290 µg/L during the intra-seismic period with an average content of ca. 35 µg/L), Ni (i.e., peak values of 33.6 and 12.5 µg/L with an average content of ca. 3 µg/L), Cr (i.e., 15 µg/L both on Nov 11 and 17, 2022 with an average abundance of 5 µg/L), Co (i.e., peak values of 1.58 and 1.34 with its average concentration being below 0.25) and Pb (i.e., displaying a maximum value of 4.50 µg/L on Nov 11, 2022 with an average content < 1 µg/L). Contrarily to the afore listed elements, V decreased during the Jun-Nov 2022 period, always showing concentrations < 1 µg/L and an average content > 2 µg/L (Fig. 4d).

Eventually, δ^2H values ranged from −49.3 ‰ to −45.2 ‰ V-SMOW (avg. −47.7 ‰, s. dev. 1.3) whereas $\delta^{18}O$ values varied from −8.55 ‰ to −7.61 ‰ V-SMOW (avg. −8.13 ‰, s. dev 0.28). Contrarily to the chemical composition, water isotopes at BET did not show any relevant change during the entire monitoring period (Table 2).

The available chemical analysis available for the CPB well field, which is pumping water from the same aquifer as the BET piezometer, carried out every six months (in May and November) by the company managing the aqueduct network (mean values reported in Table 4), showed that all the wells retained a calcium-bicarbonate composition for the last sixteen years (2006–2022) with moderate to low contents of both Na^+ and Cl^- and no notable (seasonal) variations. It is worth noticing that none of the wells displayed any chemical variations during the BET surveys. CPB wells were sampled on May 15, 2022 (i.e., before the dramatic chemical variations recorded at BET) and on Nov 13, 2022 (i.e., after the seismic event), meaning that (i) the six months gap between the two samplings did not allow to detect possible changes or (ii) the geochemical changes only affected the BET piezometer, probably due to the fact that it is located at a lower altitude with respect to the wells field or due to local characteristics of the aquifer.

4.2. *Hydrogeological characterization at BET area*

The hydrogeological characterization of the BET area was conducted through the analysis of continuous hydrogeological data, collected using hydrometric pressure transducer in the BET piezometer (daily scale), rain gauge, air temperature and TDR sensors recording data every fifteen minutes. The groundwater level at BET exhibits marked seasonal

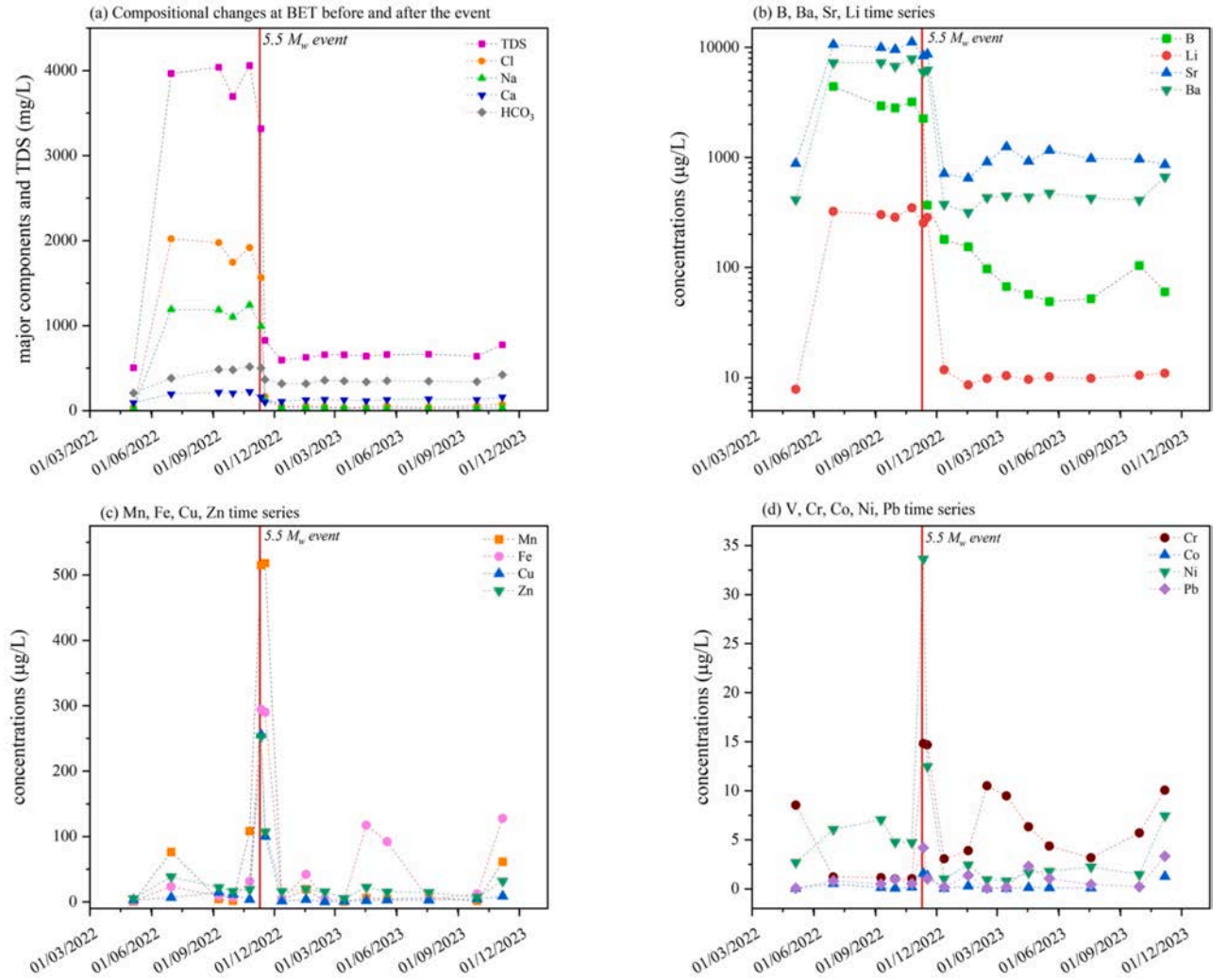

Fig. 4. Compositional variations at BET site over the May 2022 – November 2023 monitoring period: (a) major components (Ca, Na, Cl, SO_4, HCO_3) and TDS (all reported in mg/L), (b) B, Ba, Sr and Li (in µg/L), (c) Mn, Fe, Cu and Z (in µg/L) and (d) Cr, Co, Ni and Pb (in µg/L). Vertical red line indicates the day of the seismic event (November 9, 2022; $M_w = 5.5$). (For interpretation of the references to color in this figure legend, the reader is referred to the web version of this article.)

variability (Fig. 5). Minimum levels occur during late summer to autumn (Aug to Dec), while maximum levels are reached between winter and late spring (Jan to May). In absolute terms, the water table fluctuated between −1.77 and −10.8 m b.g.l., with an average value of −6.42 m. During the same period, groundwater temperature ranged between 13.3 and 16.5 °C, with an average value of 15.06 °C, showing an inverse trend compared to the fluctuations in the water table (Fig. 5).

Starting from Jan 2022, a depletion phase was observed, lasting until Jul 25, 2022. Between late Jul 2022 and Nov 15, 2022, the groundwater level remained nearly constant at approximately −9.3 m b.g.l. From mid-Nov 2022 (later than Nov 17, 2022), an effective recharge phase of the aquifer was observed under the effect of several precipitation events (Figs. 5, 6d).

The hydrological data collected form Jun 2022 to Nov 2023 at CPB are presented in Fig. 6a,b,c together with the groundwater level and temperature of BET for the same period (Fig. 6d). The graphs reveals a precipitation pattern characterized by wet conditions in winter and spring, and relatively dry periods in summer and early autumn. Summer experienced sporadic but intense rainfall events exceeding 10 mm/15 min, while wet periods entail more continuous rainfall lasting hours to days.

Air temperature ranged from zero to 35 °C throughout the hydrological year, peaking in July and reaching its lowest levels in January and February (Fig. 6a). Soil temperature mirrored that of the air trends across the monitored depths, with a lag increasing with depth. Thermal stability periods were observed in April and October 2022, March to April 2023 and October 2023 across all the soil layers. In summer, the soil temperature was higher at 0.6 m and lower at 1.7 m, while an inverse gradient occurred in winter.

Soil temperature fluctuated between 6.7 and 25.5 °C at 0.6 m, between 8.3 and 23.4 °C at 0.9 m, and from 10 to 20.8 °C at 1.7 m (Fig. 6a). Precipitation in winter led to an increase in the soil temperature at 0.6 and 0.9 m, while summer precipitation decreased it. At 1.7 m, thermal effects from infiltrating water were minimal in both seasons.

Regarding VWC (Fig. 6b), values increased after rainfall events from January to February 2022, reaching saturation in March. From March to September 2022, VWC decreased until a gradual increase in shallow soils from September, extending to deeper layers by October. By December 2022, all depths reached saturation. Hence, all the precipitation events occurring between December 2022 and May 2023 favored the increase of the groundwater level. Starting from the end of May 2023 a new recession phase was observed until November, where the

Table 4
Previous available chemical analyses for the CPB well field, which is consisting of four wells: CPBw1 to CPBw4. CPBwt refers to the loading tank collecting the waters from CPBw1, CPBw2 and CPBw3. The main statistical parameters are reported (N(analysis), mean, median, standard deviation and CV (coefficient of variation)) for pH, T (water temperature in °C), major elements and TDS (Total Dissolved Solids), in mg/L. Data are available by courtesy of VivaServizi S.p.A.

Site	Time span	Statistic	pH	T	HCO_3	F	Cl	NO_3	SO_4	Ca	Mg	Na	K	TDS
CPBwt	2006–2012	N(analysis)	12	8	12	12	12	12	12	12	12	12	12	12
		mean	7.2	14.6	319	0.3	50	27.9	42	140	10	33	1.1	623
		median	7.2	14.8	324	0.3	49	25.1	43	140	10	33	1.1	624
		std. dev.	0.1	1.0	11	0.02	3	9.8	3	5	0.5	1	0.1	22
		CV	0.02	0.07	0.03	0.03	0.06	0.39	0.07	0.04	0.05	0.03	0.10	0.03
CPBw1	2013–2023	N(analysis)	18	17	18	18	18	18	18	18	18	18	18	18
		mean	7.2	14.6	337	0.3	58	25.6	40	144	11	34	1.0	651
		median	7.2	14.7	338	0.3	53	23.2	40	144	11	32	1.0	654
		std. dev.	0.1	1.7	13	0.03	12	11.7	4	6	0.4	4	0.1	24
		CV	0.02	0.11	0.04	0.10	0.23	0.50	0.11	0.04	0.04	0.13	0.11	0.04
CPBw2	2013–2023	N(analysis)	20	19	20	20	20	20	20	20	20	20	20	20
		mean	7.2	14.9	335	0.3	54	22.1	39	142	10	33	1.1	637
		median	7.2	14.7	330	0.3	53	22.2	39	142	10	33	1.1	631
		std. dev.	0.2	1.6	14	0.02	5	6.1	4	5	0.5	2	0.1	24
		CV	0.02	0.11	0.04	0.08	0.10	0.27	0.09	0.04	0.05	0.06	0.12	0.04
CPBw3	2014–2023	N(analysis)	18	17	18	18	18	18	18	18	18	18	18	18
		mean	7.2	15.0	340	0.3	56	24.8	39	144	11	34	1.1	650
		median	7.2	14.9	340	0.3	54	23.6	39	144	11	33	1.1	648
		std. dev.	0.1	1.2	11	0.03	7	10.1	4	7	0.6	2	0.1	24
		CV	0.02	0.08	0.03	0.12	0.13	0.43	0.10	0.05	0.06	0.07	0.10	0.04
CPBw4	2013–2023	N(analysis)	14	13	14	14	14	14	14	14	14	14	14	14
		mean	7.4	16.4	227	1.0	50	8.4	35	79	6	42	4.5	679
		median	7.4	16.4	225	1.0	52	8.4	35	81	6	45	4.5	686
		std. dev.	0.12	1.0	14	0.22	9	1.3	6	7	1	12	0.3	51
		CV	0.02	0.06	0.06	0.15	0.16	0.15	0.17	0.09	0.10	0.28	0.07	0.08

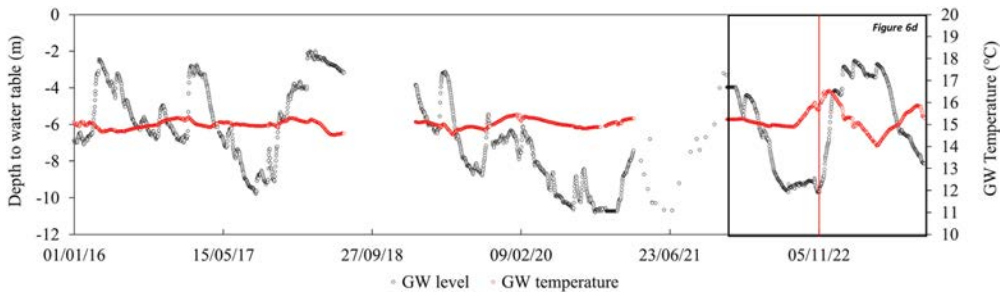

Fig. 5. Groundwater level expressed as depth to water table from the topographic surface (black dots), and groundwater temperature (red dots) over time recorded in BET at daily scale. Vertical red line indicates the day of the seismic event (November 9, 2022; Mw = 5.5). (For interpretation of the references to color in this figure legend, the reader is referred to the web version of this article.)

relatively scarce precipitation events were likely not able to supply any aquifer recharge. This aspect is also evidenced by the VWC, which only displayed an increase at 0.6 m under the effect of a single event > 10 mm/15 min that occurred in August 2023. VWC ranges from 0.22 to 0.40 m^3/m^3 at 0.6 m, 0.24 to 0.40 m^3/m^3 at 0.9 m, and 0.24 to 0.36 m^3/m^3 at 1.7 m. The bEC mirrored the VWC patterns, increasing with higher moisture levels except at 1.7 m, where sporadic infiltration events caused the decrease of bEC. The bEC ranged from 0.22 to 0.64 mS/cm at 0.6 m, 0.31 to 0.79 mS/cm at 0.9 m, and 0.24 to 1.05 mS/cm at 1.7 m (Fig. 6c). Across the sampling phase of BET, no groundwater level modifications were recorded due to the seismic event, contrarily to other case studies (e.g., Petitta et al., 2018; Barberio et al., 2020). Similarly, no marked temperature variability are registred.

5. Discussion

The geochemical composition showed no detectable changes in the MAC and VAL wells following the November 2022 seismic sequence. The low sensitivity of the sampling sites with respect to the earthquake occurrence (and the seismic cycle) was is probably related to the relatively low depth of the wells (~15 m) and the surrounding geology, since both wells are located within alluvial deposits and their waters are likely associated with shallower circulation patterns (Mattioli, 2014). However, the lack of pre-seismic chemical analysis may have limited our findings. Contrarily, major changes in multiple parameters were detected at BET piezometer starting from June 2022. It is noteworthy that the changes recorded at the BET site were transitory, meaning that pre-seismic conditions were restored following the event occurrence. This indicates that the factors/boundary conditions that produced those changes were temporary (Thomas, 1988; Cicerone et al., 2009 and references therein). Minor to major compositional variations in both major and trace elements before and concurrently with seismic events are widely reported in the literature as seismic precursory signals (e.g., Barberio et al., 2017; Hosono and Masaki, 2020; Martinelli, 2020; Gori and Barberio, 2022) and are generally associated with mixing processes, favored by the earthquake preparation processes (e.g., stress/strain changes), of two different fluids that in “steady state” conditions are hydraulically disconnected (Thomas, 1988; Cicerone et al., 2009). The strikingly strong compositional change from a low salinity Ca-HCO_3 water toward a high TDS Na-Cl facies implies that the pre-seismic Ca-HCO_3 geochemical facies was affected by a mixing process involving a high-TDS Na-Cl water. This is consistent with the widespread occurrence of highly saline connate waters trapped into the Adriatic foredeep clayey deposits like those emerging at the Aspio Terme springs, ca. 4 km

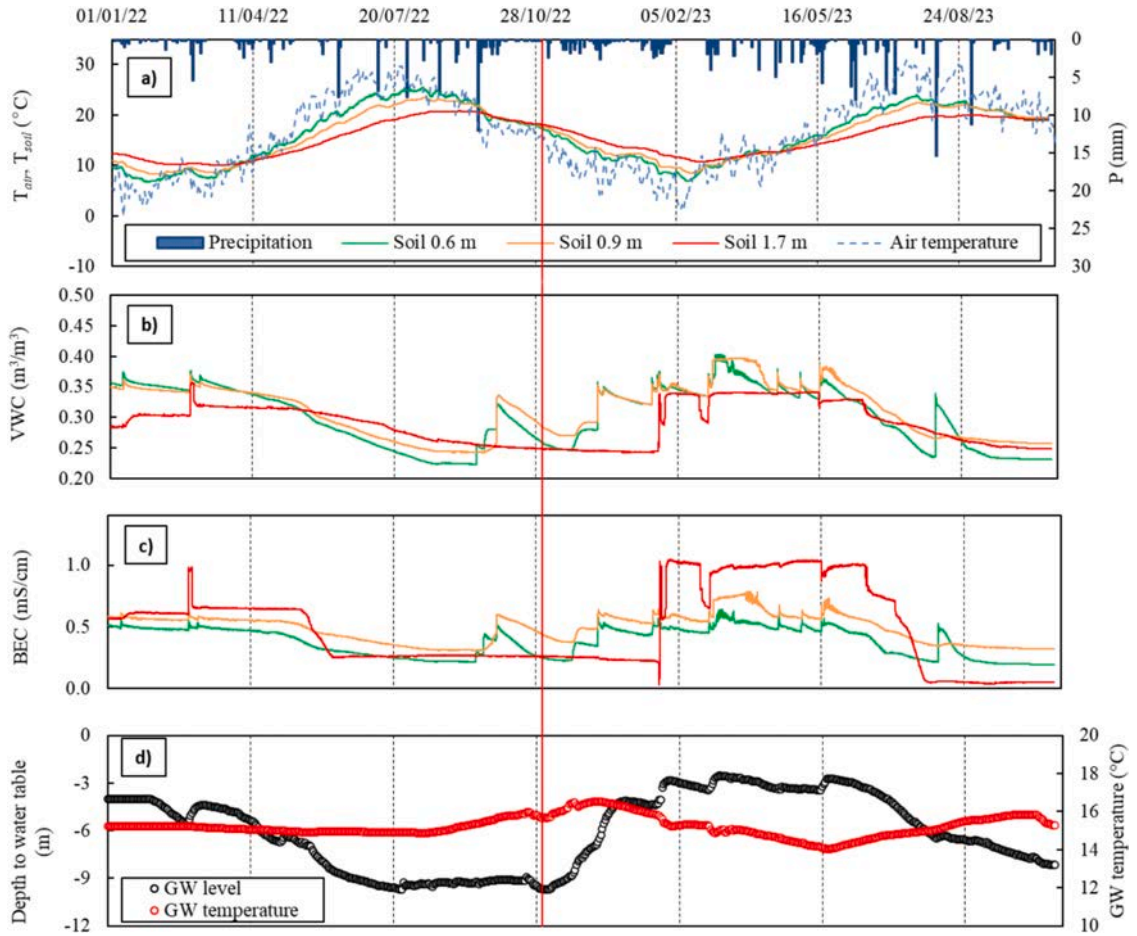

Fig. 6. Hydrogeological data collected at CPB with the TDR sensors and the thermo-pluviometric station: (a) air temperature (T_{air}), soil temperature (T_{soil}) and precipitation (P); (b) volumetric water content (VWC); (c) BEC: (d) inset of Fig. 5 relatively to groundwater level and temperature starting from January 2022. Vertical red line indicates the day of the seismic event (November 9, 2022; $M_w = 5.5$). (For interpretation of the references to color in this figure legend, the reader is referred to the web version of this article.)

eastward from the BET piezometer (Nanni and Vivalda, 1999). These waters are characterized by a sodium-chloride facies, with Cl contents up to ~ 10,000 mg/L Na ~ 4500 mg/L and TDS ~ 17,000 mg/L (Nanni and Vivalda, 1999), hence representing a possible saline end-member. Furthermore, EC-logs performed at the BET piezometer showed a stratification of the aquifer (Fig. 7) with relatively low EC (< 1000 μS/cm) in the first 6–7 m below the saturation level, followed by a sharp increase of EC (up to 6500–7000 μS/cm) in the subsequent 9–10 m (down to 22–23 m b.g.l) and a last increase up to ~ 25,000 μS/cm towards the bottom of the piezometer. This confirms the presence of an "Aspio-like" end-member underneath BET.

Taking this into account, a two-component chemical mixing model was developed by using the geochemical code PHREEQC 3.7.3–15968 (wateq4f.dat database; Parkhurst and Appelo, 2013) with the aim of verifying whether the observed outstanding BET chemical variation between June and November 2022 (Table 2) was due to a mixture between the typical BET Ca-HCO_3 composition recognized in the shallower parts of the aquifer and the more saline waters characterizing the bottom of piezometer column (Fig. 7). The sample BET Jan 17, 2023 (Table 2), i.e., when chemical concentrations recovered their usual low values, was selected as the first end-member. On the other hand, since no data of the deeper part of the aquifer is available, the average composition based on available analytical data of samples from the nearby Na-Cl thermal springs of Aspio Terme (e.g., Nanni and Vivalda, 1999; Table S1) was included as the targeted end-member.

The simulation was run considering the major available ions, the temperature and pH values of the two solutions, while the redox conditions were related to the value of pe (conventional negative log of the activity of the electron, expression of the oxidation-reductive state; Parkhurst and Appelo, 2013), which was calculated from the available Eh values based on the formula (Thorstenson, 1984, Yadav et al., 2020):

$$pe = (F/2.303RT) \times Eh$$

where F is Faraday's constant, 2.303 is the conversion factor between log and ln, R the universal gas constant, T the temperature (K), and Eh, the measured redox potential. Focusing on the main anion (Cl) and cation (Na), which can be considered as useful geochemical tracers, the result of the simulation shows that the BET mean water composition between June and November 2022 can be reproduced by mixing the Ca-HCO_3 and Na-Cl endmembers by ~ 75 %–25 %, respectively (Fig. 8). This is consistent with the interpretation of an Aspio-like saline input at the bottom of the BET piezometer that enhanced the considerable compositional change observed. This input was followed by a complete recovery of the previous conditions.

The occurrence of the mixing process is also supported by the structural features of the study area. During the inter-seismic stage, the "Aspio-like" saline waters were detected at the BET piezometer bottom (Fig. 7) (>22–23 m) where the marly limestones of the Schlier Fm were

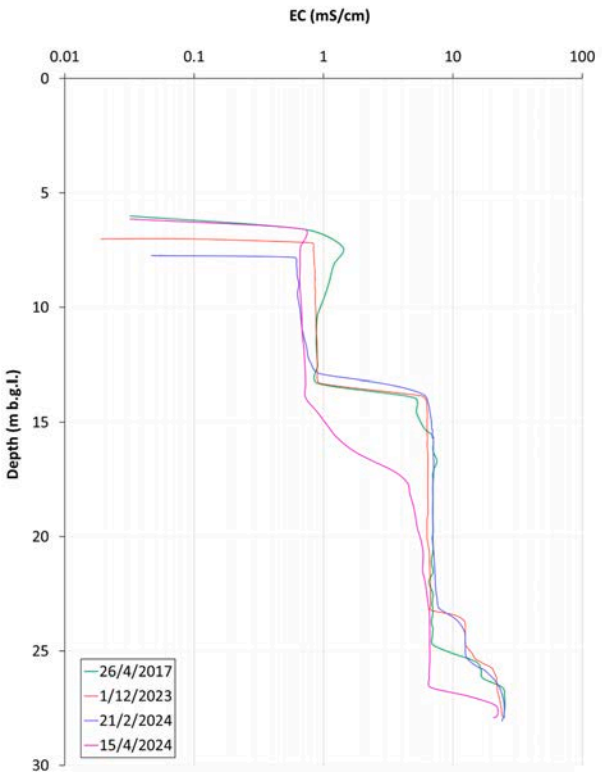

Fig. 7. Electrical conductivity (EC) vertical logs performed at the BET piezometer on April 2017, on December 2023, February and April 2024, showing the presence of a deeper and more saline water located at the bottom of the piezometer.

encountered. Recent studies indicate that significant fracture-related permeability characterizes this formation in the study area (conductivity K: 2.9 × 10^{-3} cm/s), where it behaves as a subsidiary aquifer (Mammoliti et al., 2023). Therefore, during inter-seismic times, "Aspio-like" saline waters characterize a deeper aquifer hosted in the upper (i.e., Miocene) part of the pre-Quaternary substratum, while low salinity waters occupy a shallow aquifer hosted in the surficial alluvial deposits (Fig. 2c).

During the monitoring phase, wet periods are associated with a general increase in bEC across various levels of the unsaturated zone within the alluvial aquifers (Fig. 6c). This trend suggests the possible mineralization of rainwater infiltrating into the aquifer. Notably, the highest bEC values recorded at a depth of 1.7 m (approximately 1.0 mS/cm) are comparable to those found in the uppermost portion of the aquifer (Fig. 7), indicating that "Aspio-like" waters are hosted in the upper Miocene section of the pre-Quaternary substratum, and are not the result of meteoric recharge and direct infiltration processes.

Furthermore, a pumping test was conducted at BET on Mar 17, 2024 (Fig. S1), involving groundwater extraction at a constant rate of 0.56 l/s for 3 h using a pump positioned at 15 m b.g.l. Throughout the test, the extracted groundwater temperature remained constant at 15.1 °C, while the EC increased linearly from an initial value of 0.82 mS/cm to 1.51 mS/cm in the first hour. Subsequently, the EC rose slightly up to 1.8 mS/cm over the next 1 h and 20 min and then stabilized until the test concluded. The groundwater level exhibited an exponential decline from 6.26 m b.g.l. to 9.02 m b.g.l. within the first 30 min, following a linear decrease for the remaining 2 h and 30 min, reaching a minimum level of 10.75 m b.g.l. The water level recovered rapidly within approximately 10 min once the pumping was shut down.

The observed dynamics of the alluvial aquifers, as elucidated by the pumping test, suggest that during inter-seismic periods and under natural conditions, water circulation is primarily sustained by high permeability lenses and layers between 10 and 16 m b.g.l., consisting of alternating gravel and sandy gravel, confined both above and below by thick deposits of clay and silts (Fig. 2c) (Kim et al., 2005; Zappa et al., 2006). The gravelly and sandy-gravel layers, characterized by high-permeability, are responsible for recharging the piezometer without drawing groundwater from the deeper zones within the fracture-related permeable Miocene bedrock (i.e., Schlier Fm) (Mammoliti et al., 2023), thus not involving the "Aspio-like" water type. Such configuration makes the piezometer itself a hydraulic connection between the bedrock and the overlying aquifer hosted in the Quaternary deposits. This evidence also supports the interpretation that no marked changes in groundwater level within the piezometer occurred during the seismic phase, since the upward-moving groundwater amount from the substrate to the alluvial aquifer may have been easily dissipated by the more permeable lenses and layers. The presence of low-permeability beds composed by clayey silts (between 16 and 21 m b.g.l.; Fig. 2c), which naturally separate the substrate from the gravel and sandy layers of the

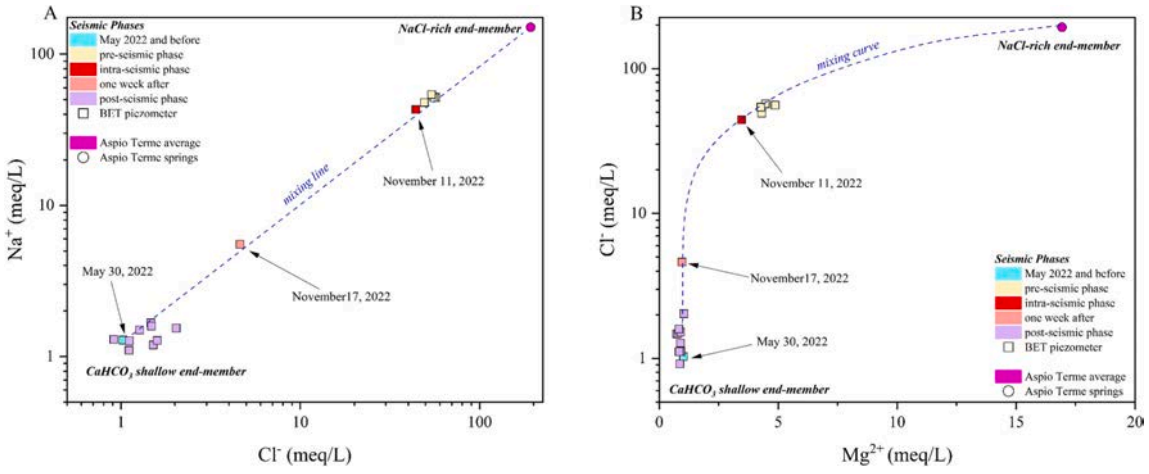

Fig. 8. Two-component geochemical mixing model: (a) Na^+ vs. Cl^- binary diagram and (b) Cl^- vs. Mg^{2+} binary diagram. All values are reported in meq/L. Water samples are coloured according to the time of sampling (i.e., pre-seismic, intra-seismic and post-seismic). The Aspio Terme average composition is considered as the second mixing end-member (Nanni and Vivalda, 1999). See the text for further details.

Quaternary deposits (Fig. 2c), has prevented the diffuse upward migration of the "Aspio-like" water to the entire alluvial aquifer. This is consistent with that observed in the shallow CPB wells that do not reach the substrate, and thus prevent the hydraulic connection between the two identified groundwater circulations.

To further discuss the possible dynamics of pre-seismic mixing of these two-water types, we must consider the tectonic setting of the pre-Quaternary substratum in the region. The outer portion of the Apennine fold and thrust belt in the Marche offshore is compartmentalized by transversal faults (Fig. 1). Although ca. 50 km apart, the November 9, 2022 earthquake epicenter and the BET piezometer site are located within the same crustal block of the fold and thrust belt. It is well known that the small strains characterizing areas far (>50 km) from the earthquake foci are sufficient to trigger mixing of groundwater sources during the preparatory stages of medium-size earthquakes ($5.3 \leq M \leq 5.8$, e.g., Skelton et al., 2019). The fundamental role of microfractures has been proposed to control such a mixing, which would reflect slow leakage along a fracture system (Claesson et al., 2004).

In the present study, the occurrence of mixed waters was recorded in the upper (alluvial deposits) section of the BET piezometer. Therefore, this section of the piezometer must have been invaded by more saline ("Aspio-like") waters migrated from deeper levels until its shallower portion involving an intra-borehole transport effect (Zinn and Konikow, 2007). This means that the opening of fluid pathways (i.e., dilatational microfractures) in the pre-Quaternary substratum was accompanied by the upward flow of over-pressured water from a deeper reservoir, hosted in the Schlier Fm and experiencing horizontal compression, which is consistent with the regional tectonic setting of thrust earthquakes. It may be envisaged that during the preparatory phase of the earthquake (i.e., the pre-seismic stage, which started a few months before the mainshock), the crustal volume hosting both the earthquake foci and the BET piezometer experienced enhanced horizontal bulk shortening. This would have led to the buildup of horizontal compressive stress in the Meso-Cenozoic substratum units, including the Miocene formations of Mt. Conero. The main fracture systems detected in the Schlier Fm include both parallel and perpendicular sets to the active NW-NE-oriented shortening (Fig. 2d) (Mammoliti et al., 2023). While part of the fracture network (i.e., NW striking subvertical structures) experienced compression and tightening, favorably oriented structures underwent dilation, and further microfractures formed during the pre-seismic stage. Within this framework, overall conditions of fluid overpressure are interpreted to have triggered fluid expulsion and upward flow within the BET piezometer, leading to a mixing with near-surface waters within the alluvial deposits hosting the shallow aquifer. Such overpressure conditions were maintained in the fractured beds of the Schlier Fm (Fig. 2d) until November 9, 2022 when stress release following the main seismic event(s) led to the reestablishment of normal pressure conditions in the deeper reservoir.

The restoration of the hydrochemical conditions to the bicarbonate-calcium facies after the mainshock is not evidently related to neither meteoric dilution nor direct recharge processes, which started only from the second half of November 2022 onwards as evidenced by the groundwater level increase (Fig. 4).

A key issue in the foregoing interpretation is that "Aspio-like" saline waters are hosted in the pre-Quaternary substratum rocks able to experience tectonic strain associated with thrust fault loading during the pre-seismic stage. The nearby CPB wells, which were not able to connect deep and shallow aquifers because of their limited depths (not reaching substratum lithologies), did not record any variability in terms of water chemistry. This feature confirms that the variations observed in the BET piezometer are a result of fluid flow and interactions internal to – and controlled by – borehole dynamics. In the lack of any borehole connection (e.g., CPB wells), no mixing occurred between shallow and deep waters hosted in alluvial deposits and substratum lithologies, respectively.

Further evidence that needs to be considered is the differential behavior detected for trace elements (Fig. 4b, c, d). Boron, Sr, Ba and Li increased concurrently with the TDS and the Na-Cl composition, while the transition metals showed their peak values on November 11 and November 17, 2022 (i.e., two days and one week after the seismic event). To investigate this different behavior, a comparison was made between the concentrations of the dissolved trace elements and those contained in the rock that is assumed to constitute the basement below BET, i.e., the Schlier Fm. The assumptions of this elaboration were, as follows: i) the BET selected waters were those of June 30, 2022 ("Aspio-like" saline waters), the November 11, 2022 and November 17, 2022 (i.e., in close proximity to the earthquake), and the July 19, 2023 ("normal-BET" water); ii) the selected rock was taken from Mader et al. (2004), which determined the chemical composition of an interval of the nearby Schlier marly limestone sequence of La Vedova (Conero, Ancona, Italy), by choosing a sample with "marly limestone" composition (v22.3) and with the greatest amount of analyzed trace elements; iii) both water and rock composition (considering the analyzed elements available in both matrices) were normalized to the primitive mantle (PM) composition (from Palma and O'Neill, 2004) in order to be compared (Cabassi et al., 2019). Unfortunately, some elements (i.e., B, Li, Pb) were not available for the rock, therefore it was not possible to include them in this modeling. The resulting spider diagram of Fig. 9 shows that Ba, Sr and Rb, which are commonly efficiently mobilized by water–rock interaction processes (e.g., Middelburg et al., 1988; Dequincey et al., 2002; Cabassi et al., 2014), display higher concentrations than those in the "normal-BET" water even before the earthquake. In fact, no substantial difference can be appreciated between the June 30, 2022, and the two November 2022 samples. Consequently, as also confirmed by the Arsenic content (more concentrated in the June 30, 2022 water), they were likely present in the "Aspio-like" end-member (Nanni and Vivalda, 1999, 2005) and involved in the mixing process that occurred in the pre-seismic phase, i.e., during the buildup of the horizontal compressive stress. On the other hand, transition metals (Cr, Mn, Fe, Co, Ni, Cu, Zn, with the only exception of V), generally characterized by lower mobility (e.g., Kaasalainen et al., 2015; Cabassi et al., 2019), displayed a striking difference (up to two orders of magnitude for Fe, Mn and Cu; Fig. 9) between pre-, inter- and post-earthquake periods. They are significantly more concentrated in the November 2022 water samples and show a water/PM ratio closer to the rock/PM one with respect

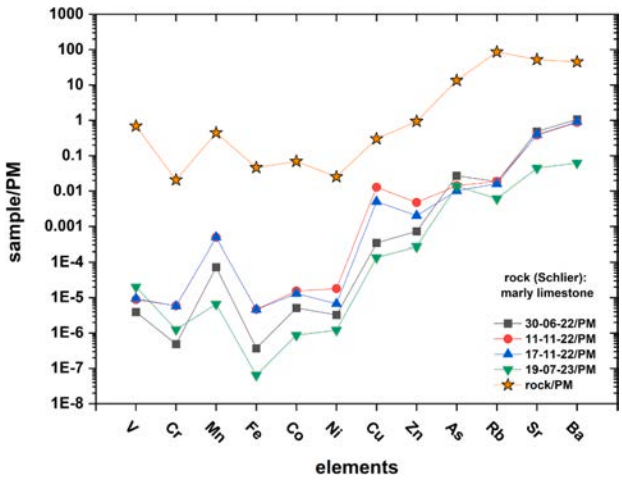

Fig. 9. Normalized concentrations of V, Cr, Mn, Fe, Co, Ni, Cu, Zn, As, Rb, Sr and Ba to the Earth primitive mantle (PM) (Palme and O'Neill, 2014) for the BET selected waters (i.e., June 30, 2022, November 11, 2022, November 17, 2022 and July 19, 2022) compared with those measured in a rock sample with "marly limestone" composition (v22.3) belonging to the Schlier sequence of La Vedova (Conero, Ancona, Italy; Mader et al., 2004). See the text for further details.

to both "normal-BET" and "Aspio-like" waters. Such evidence suggests that the origin of the anomalous concentrations may not be related to the mixing processes but rather to a different mechanism involving the local lithologies, as confirmed by the waters approaching trend towards the rock elemental values. Among the available literature (King et al., 1994; Cicerone et al., 2009 and therein references), the physical mechanisms of the *unclogging of the flow paths* following a seismically-induced permeability enhancement concurrently to moderate-to-strong earthquakes is widely documented. According to the proposed mechanism (King et al., 1994; Barbosa et al., 2019; 2020), the stress release after the mainshock may have produced an increase in the fractures' permeability, thus favoring the fluid mobility within the Schlier fractured formation. The fracture unclogging may have determined the mobilization of the deposited colloids and clasts in the fractures and veins network within the Schlier Fm, which were taken over by the fluid and flowed into the piezometer (Barbosa et al., 2019). The occurrence of such a process was not only supported by the geochemical evidence and modeling (Fig. 9) but also by the observation that during the sample collection on November 11, 2022, the BET water was characterized by high turbidity and a brownish color.

Therefore, the striking hydrogeochemical variations recorded at BET were possibly related to two different seismically-induced processes: (i) the first one occurring during the pre-seismic stage and related to the earthquake preparation process and the stress buildup which determined the mixing between the shallow (Ca-HCO_3) and the deep (Na-Cl) waters, and (ii) the second one occurring concurrently with the earthquake which increased the hydraulic conductivity in the Schlier Fm and favored fracture unclogging.

6. Conclusions

In this study, we presented the results of a pre- and post-seismic water monitoring network deployed in the Mt. Conero area following the November 9, 2022 seismic sequence of the Adriatic offshore and aimed at evaluating the possible influence of the seismic event on the water geochemistry and understanding the underlying physical and chemical mechanisms. Among the three surveyed sampling sites selected, VAL and MAC did not show any significant variations following the event since these waters are probably related to shallow hydrological pathways with limited water–rock interactions. On the contrary, the BET piezometer displayed remarkable hydrogeochemical changes starting from ~ 4 months before the event. In fact, since the end of June 2022, we detected a compositional change from a Ca-HCO_3 to Na-Cl geochemical facies at which corresponded a strong increase (ca. 350 %) in the TDS content (from < 1000 mg/L up to more than 3500 mg/L). About a week after the seismic sequence the geochemical composition to Ca-HCO_3 was restored. Striking changes, up to 50 times their average contents, were also detected in the trace element contents with (i) B, Sr, Li, Ba and Rb showing increments from June 2022 whereas (ii) the transition metals (e.g., Fe, Mn, Cu) peaking in those samples collected following the mainshocks.

The hydrogeochemical and structural evidence presented indicate that the BET piezometer was affected by the occurrence of two seismically-induced processes which determined the detected compositional changes. Specifically, during the earthquake preparation process (pre-seismic stage), the buildup of horizontal compressive stress, favored the uprise of deep and saline Na-Cl waters located in the substratum that hosts the BET piezometer and determined a mixing with the shallow Ca-HCO_3 waters. The occurrence of such a process can explain – and constrain – the origin of the compositional change detected since June 2022. Immediately following the mainshocks, the stress release led to an enhancement in fracture permeability, which increased the fluid mobility within the Schlier Fm driving to fracture unclogging. This process allowed the mobilization of the material contained within the fractures and veins, which interacting with the fluid, increased the transition metal contents (Fig. 9).

The hydrogeochemical changes observed at the BET piezometer are among the most clear and evident ever reported and proved the high sensitivity of hydrogeochemical monitoring to record pre-seismic variations. This makes these sampling sites extremely interesting and worth of continuous monitoring, since the Adriatic Sea offshore is frequently affected by moderate seismicity. On the other hand, the absence of variation recorded at VAL and MAC wells, which are located in the same area and only a few kilometers away from the BET piezometer, again proves the extreme difficulty in finding suitable and sensitive monitoring sites, since local structural or lithological features may make a site insensitive and therefore unsuitable for seismic surveillance. With this framework, the peculiar configuration of the BET, being able to hydraulically connect two groundwater circulations – the lower one sustained by fractures in the substrate, and the upper one involving the alluvial aquifer, each of one marked by its own hydrogeochemical facies – may provide a useful example for the design of appropriate sites of hydrogeochemical monitoring of seismic activity. In the future, the implementation of an equipped piezometer with real-time data transmission, connecting the substrate (also for depths greater than those reached by BET) with the shallow (alluvial) aquifers, in an area of such high tectonic stress, could represent a promising action to be addressed in the field of seismic surveillance.

CRediT authorship contribution statement

Lorenzo Chemeri: Writing – review & editing, Writing – original draft, Visualization, Validation, Methodology, Investigation, Formal analysis, Data curation, Conceptualization. **Marco Taussi:** Writing – review & editing, Writing – original draft, Visualization, Validation, Supervision, Methodology, Investigation, Conceptualization. **Davide Fronzi:** Writing – review & editing, Writing – original draft, Validation, Methodology, Investigation, Formal analysis, Data curation, Conceptualization. **Jacopo Cabassi:** Writing – review & editing, Writing – original draft, Validation, Investigation, Data curation, Conceptualization. **Stefano Mazzoli:** Writing – review & editing, Writing – original draft, Validation, Investigation, Conceptualization. **Alberto Tazioli:** Writing – review & editing, Supervision, Resources. **Alberto Renzulli:** Writing – review & editing, Supervision, Resources. **Orlando Vaselli:** Writing – review & editing, Supervision, Resources.

Declaration of competing interest

The authors declare that they have no known competing financial interests or personal relationships that could have appeared to influence the work reported in this paper.

Acknowledgments

LC was financially supported by University of Urbino Carlo Bo through a ReMeST PhD Grant (XXXVII cycle) until 31 October 2024 and a postdoc position since November 2024. The authors would like to thank Dr. F. Capecchiacci and Dr. C. Macelli for their help in the analytical analysis performed at the Department of Earth Sciences, University of Florence. The authors also thank VivaServizi S.p.A for providing the available chemical analysis of the well field and for allowing the placement of instrumentation for monitoring. Dr. S. Palpacelli is thanked for the help provided during the instruments installation on the field. The three anonymous reviewers and the editor (C. Corradini) are greatly thanked for their comments and suggestions that helped us to improve the manuscript.

Appendix A. Supplementary data

Supplementary data to this article can be found online at https://doi.org/10.1016/j.jhydrol.2025.132792.

Data availability

Data will be made available on request.

References

Barberio, M.D., Barbieri, M., Billi, A., Doglioni, C., Petitta, M., 2017. Hydrogeochemical changes before and during the 2016 Amatrice-Norcia seismic sequence (central Italy). Sci. Rep. 7 (1), 11735.

Barberio, M.D., Gori, F., Barbieri, M., Billi, A., Caracausi, A., De Luca, G., Franchini, S., Petitta, M., Doglioni, C., 2020. New observations in Central Italy of groundwater responses to worldwide seismicity. Sci. Rep. 10, 17850.

Barbosa, N.D., Hunziker, J., Lissa, S., Saenger, E.H., Lupi, M., 2019. Fracture unclogging: a numerical study of seismically induced viscous shear stresses in fluid-saturated fractured rocks. JGR Solid Earth 124 (11), 11705–11727.

Barbosa, N.D., Solazzi, S.G., Lupi, M., 2020. Seismically induced unclogging in fluid-saturated faults. JGR Solid. Earth 125 (8), e2020JB020152.

Barchi, M.R., Mirabella, F., 2009. The 1997-98 Umbria-Marche earthquake sequence: "Geological" vs. "seismological" faults. Tectonophysics 476 (1–2), 170–179.

Barchi, M., Alvarez, W., Shimabukuro, D.H., 2012. The Umbria-Marche Apennines as a double orogen: observations and hypothesis. It. J. Geosci. (boll. Soc. Geol. It) 131, 258–271.

Basili, R., Barba, S., 2007. Migration and shortening rates in the northern Apennines, Italy: implications for seismic hazard. Terra Nova 19 (6), 462–468.

Bonini, M., Corti, G., Delle Donne, D., Sani, F., Piccardi, L., Vannucci, G., Genco, R., Martelli, L., Ripepe, M., 2016. Seismic sources and stress transfer interaction among axial normal faults and external thrust fronts in the Northern Apennines (Italy): a working hypothesis based on the 1916-1920 time-space cluster of earthquakes. Tectonophysics 680, 67–89.

Boschetti, T., Barbieri, M., Barberio, M.D., Billi, A., Franchini, S., Petitta, M., 2019. CO2 inflow and elements desorption prior to a seismic sequence, Amatrice-Norcia 2016, Italy. Geochem. Geophys. Geosyst. 20, 2303–2317.

Busico, G., Colombiani, N., Fronzi, D., Pellegrini, M., Tazioli, A., Mastrocicco, M., 2020. Evaluating SWAT model performance, considering different soils data input, to quantify actual and future runoff susceptibility in a highly urbanized basin. J. Env. Man. 265, 110625.

Busico, G., Fronzi, D., Colombiani, N., Mastrocicco, M., Tazioli, A., 2024. Identification and quantification of nutrients sources in the Aspio watershed (Italy). Insight from geogenic mineralization and anthropogenic pressure. Catena 263, 107759.

Butler, R. H. W., Mazzoli, S., Corrado, S., De Donatis, M., Di Bucci, D., Gambini, R., Naso, G., Nicolai, C., Scrocca, D., Shiner, P., Zucconi, V., 2004. Applying thick-skinned tectonic models to the Apennine thrust belt of Italy – limitations and implications. In K. R. McClay (Ed.), Thrust tectonics and hydrocarbon systems (Vol. 82, pp. 647-667). AAPG Memoir.

Cabassi, J., Capecchiacci, F., Magi, F., Vaselli, O., Tassi, F., Montalvo, F., Esquivel, I., Grassa, F., Caprai, A., 2019. Water and dissolved gas geochemistry at Coatepeque, Ilopango and Chanmico volcanic lakes (El Salvador, Central America). J. Volcanol. Geoth. Res. 378, 1–15.

Cabassi, J., Tassi, F., Mapelli, F., Borin, S., Calabrese, S., Rouwet, D., Chiodini, G., Marasco, R., Chouaia, B., Avino, R., Vaselli, O., Pecoraino, G., Capecchiacci, F., Bicocchi, G., Caliro, S., Ramirez, C., Mora-Amador, R., 2014. Geosphere-biosphere interactions in bio-activity volcanic lakes: evidences from Hule and Rio Cuarto (Costa Rica). PLoS One 9 (7), e102456.

Calamita, F., Deiana, G., Invernizzi, C., Pizzi, A., 1991. Tettonica. In: L'ambiente fisico delle Marche, 67-80. Ed. SELCA, Firenze.

Calamita, F., Pizzi, A., 1994. Recent and active extensional tectonics in the southern Umbro-Marchean Apennines (Central Italy). Mem. Soc. Geol. It. 48, 541–548.

Cambi, C., Mirabella, F., Petitta, M., Banzato, F., Beddini, G., Cardellini, C., Fronzi, D., Mastrorillo, L., Tazioli, A., Valigi, D., 2022. Reaction of the carbonate Sibiliini Mountains basal aquifer (Central Italy) to the extensional 2016-2017 seismic sequence. Sci. Rep. 12, 22428.

Cello, G., Tondi, E., 2014. Note illustrative della carta geologica d'Italia alla scala 1: 50.000. Foglio 282. Ancona. ISPRA-Roma.

Chemeri, L., Taussi, M., Cabassi, J., Capecchiacci, F., Randazzo, A., Tassi, F., Renzulli, A., Vaselli, O., 2024. Groundwater and dissolved gases geochemistry in the Pesaro-Urbino Province (northern Marche, central Italy) as a tool for seismic surveillance and sustainability. Sustainability 16, 5178.

Chicco, J., Pierantoni, P.P., Costa, M., Invernizzi, C., 2019. Plio-Quaternary tectonics and possible implications for geothermal fluids in the Marche Region (Italy). Tectonophysics 755, 21–34.

Chiodini, G., Cardellini, C., Di Luccio, F., Selva, J., Frondini, F., Caliro, S., Rosiello, A., Beddini, G., Ventura, G., 2020. Correlation between tectonic CO2 earth degassing and seismicity is revealed by a 10-year record in the Apennines, Italy. Science. Advances 6 (35), eabc2938.

Cicerone, R.D., Ebel, J.E., Britton, J., 2009. A systematic compilation of earthquake precursors. Tectonophysics 476, 371–396.

Cinti, D., Sciarra, A., Cantucci, B., Galli, G., Pizzino, L., Procesi, M., Poncia, P.P., 2023. Hydrogeochemical investigations of shallow aquifers before and after the 2012 Emilia seismic sequence (northern Italy). Appl. Geochem. 151, 105624.

Claesson, L., Skelton, A., Graham, C., Dieti, C., Mörth, C.-M., Torssander, P., Kockum, I., 2004. Hydrogeochemical changes before and after a major earthquake. Geology 32, 641–644.

Copley, E., Hollingsworth, J., Bergman, E., 2012. Constrains on fault and lithosphere rheology from the coseismic slip and postseismic afterslip of the Mw 7.0 Mozambique earthquake. JGR: Solid. Earth 117 (83).

Coward, M.P., De Donatis, M., Mazzoli, S., Paltrinieri, W., Wezel, F.C., 1999. Frontal part of the northern Apennines fold and thrust belt in the Romagna-Marche area (Italy): shallow and deep crustal styles. Tectonics 18, 559–574.

Dequincey, O., Chabaux, F., Clauer, N., Sigmarsson, O., Liewig, N., Leprun, J.C., 2002. Chemical mobilizations in laterites: evidence from trace elements and 238U-234U-230Th disequilibria. Geochim. Cosmochim. Acta 66 (7), 1197–1210.

Dewey, J. F., Helman, M. L., Turco, E., Hutton, D. H. W., Knott, S. D., 1989. Kinematics of the western Mediterranean. In: Coward, M. P., Dietrich, D., Park, R. G., (eds) Alpine Tectonics, Geological Society, London, Special Publications, 45, 265-283.

DISS Working Group, 2021. Database of Individual Seismogenic Sources (DISS), Version 3.3.0: a compilation of potential sources for earthquakes than M 5.5 in Italy and surrounding areas. Istituto Nazionale Di Geofisica e Vulcanologia (INGV).

Doglioni, C., Barba, S., Carminati, E., Riguzzi, F., 2014. Fault on-off versus coseismic fluid reactions. Geosci. Front. 5 (6), 767–780.

Doglioni, C., 1995. Geological remarks on the relationships between extension and convergent geodynamic setting. Tectonophysics 252 (1–4), 253–267.

Fantoni, R., Franciosi, R., 2010. Tectono-sedimentary setting of the Po Plain and Adriatic foreland. Rendiconti Lincei- Scienze Fisiche e Naturali 21, 197–209.

Franchini, F., Agostini, S., Barberio, M.D., Barbieri, M., Billi, A., Boschetti, T., Pennisi, M., Petitta, M., 2021. HydroQuakes, central Apennines: towards a hydrogeochemical monitoring network for seismic precursors and the hydro-seismo-sensitivity of boron. J. Hydrol. 598, 125754.

Fronzi, D., Banzato, F., Caliro, S., Cambi, C., Cardellini, C., Checcucci, R., Mastrorillo, L., Mirabella, F., Petitta, M., Valigi, D., Tazioli, A., 2020a. Preliminary results on the response of some springs of the Sibillini Mountains area to the 2016-2017 seismic sequence. Acque Sotterranee-Italian Journal of Groundwater.

Fronzi, D., Di Curzio, D., Rusi, S., Valigi, D., Tazioli, A., 2020b. Comparison between periodic tracer tests and time-series analysis to assess mid-and long-term recharge model changes due to multiple strong seismic events in carbonate aquifers. Water 12 (11), 3073.

Fronzi, D., Gaiolini, M., Mammoliti, E., Colombani, N., Palpacelli, S., Marcellini, M., Tazioli, A., 2022. Groundwater-surface water interaction revealed by meteorological trends and groundwater fluctuations on stream water level. Acque Sotterranee-Italian Journal of Groundwater 11 (2), 19–28.

Fronzi, D., Mirabella, F., Cardellini, C., Caliro, S., Palpacelli, S., Cambi, C., Valigi, D., Tazioli, A., 2021. The role of faults in groundwater circulation before and after seismic events: Insights from tracers, water isotopes and geochemistry. Water 13 (11), 1499.

Fronzi, D., Narang, G., Galdelli, A., Pepi, A., Mancini, A., Tazioli, A., 2024. Towards Groundwater-Level Prediction Using Prophet Forecasting Method by Exploiting a High-Resolution Hydrogeological Monitoring System. Water 16 (1), 152.

Gori, F., Barberio, M.D., 2022. Hydrogeochemical changes before and during the 2019 Benevento seismic swarm in central-southern Italy. J. Hydrol. 604, 127250.

Hosono, T., Masaki, Y., 2020. Post-seismic hydrochemical changes in regional groundwater flow systems in response to the 2016 Mw 7.0 Kumamoto earthquake. J. Hydrol. 580, 124340.

Hosono, T., Yamada, C., Manga, M., Wang, C.-Y., Tanimizu, M., 2020. Stable isotopes show that earthquakes enhance permeability and release water from mountains. Nat. Commun. 11, 1–9.

Hosono, T., Yamada, C., Shibata, T., Tawara, Y., Wang, C.-Y., Manga, M., Rahman, A.T. M.S., Shimada, J., 2019. Coseismic groundwater drawdown along crustal ruptures during the 2016 Mw 7.0 Kumamoto earthquake. Water Resour. Res 55, 5891–5903.

ISPRA, 2011. Note illustrative della carta geologica d'Italia, Foglio 293, Osimo.

Kaasalainen, H., Stefánsson, A., Giroud, N., Arnórsson, S., 2015. The geochemistry of trace elements in geothermal fluids, Iceland. Appl. Geochem. 62, 207–223.

Keller, J.V.A., Minelli, G., Pialli, G., 1994. Anatomy of late orogenic extenstion: the Northen Apennine case. Tectonophysics 238 (1–4), 275–294.

Kim, J.W., Choi, H., Lee, J.Y., 2005. Characterization of hydrogeologic properties for a multi-layered alluvial aquifer using hydraulic and tracer tests and electrical resistivity survey. Environ. Geol. 48, 991–1001.

King, C.-Y., 1986. Gas geochemistry applied to earthquake prediction: an overview. J. Geophys. Res. 91, 12269–12281.

King, C.-Y., Basler, D., Presser, T.S., Evans, W.C., Minissale, A., 1994. In search of earthquake related hydrologic and chemical changes along Hayward fault. Appl. Geochem. 9, 83–91.

Kitagawa, Y., Koizumi, N., Takahashi, M., Matsumoto, N., Sato, T., 2006. Changes in groundwater levels or pressures associated with the 2004 earthquake off the west coast of northern Sumatra (M9.0). Earth Planets Space 58, 173–179.

Köppen, W., Geiger, R., 1954. Klima der Erde (Climate of the earth). Wall Map 1:16 Mill. Klett-Perthes, Gotha.

Lavecchia, G., Boncio, P., Creati, N., 2003. A lithospheric-scale seismogenic thrust in Central Italy. J. Geodyn. 36, 79–94.

Lavecchia, G., Barchi, M., Brozzetti, F., Menichetti, M., 1994. Sismicità e tettonica nell'area umbro-marchigiana. Boll. Soc. Geol. It. 113, 483–500.

Lee, H.A., Hamm, S.-Y., Woo, N.C., 2017. Groundwater monitoring network for earthquake surveillance and prediction. Econ. Environ. Geol 50, 401–414.

Lee, H.A., Hamm, S.-Y., Woo, N.C., 2021. Pilot-scale groundwater monitoring network for earthquake surveillance and forecasting research in Korea. Water 13, 2448.

Mader, D., Koeberl, C., Montanari, A., 2004. Geochemistry of a Langhian pelagic marly limestone sequence of the Conero Riviera, Ancona (Italy) and the search for a Ries impact signature: a progress report. In: Cratering in Marine Environments and on Ice. Berlin, Heidelberg, Springer, Berlin Heidelberg, pp. 149–184.

Maesano, F. E., Buttinelli, M., Maffucci, R., Toscani, G., Basili, R., Bonini, L., Burrato, P., Fedorik, J., Fracassi, U., Panara, Y., Tarabusi, G., Tiberti, M. M., Valensise, G., Vallone, R., Vannoli, P., 2023. Buried alive: imaging of the 9 November 2022, M2 5.5 earthquake source on the Offshore Adriatic blind thrust front of the Northern Apennines (Italy). Geophysical Research Letters, 50, e2022GL102299.

Mammoliti, E., Fronzi, D., Cambi, C., Mirabella, F., Cardellini, C., Patacchiola, E., Tazioli, A., Caliro, S., Valigi, D., 2022. A holistic approach to study groundwater-surface water modifications induced by strong earthquakes: The case of Campiano catchment (Central Italy). Hydrology 9 (6), 97.

Mammoliti, E., Pepi, A., Fronzi, D., Morelli, S., Volatili, T., Tazioli, A., Francioni, M., 2023. 3D discrete fracture network modelling from UAV imagery coupled with tracer tests to assess fracture conductivity in an unstable rock slope: implications for rockfall phenomena. Remote Sens. (Basel) 15, 1222.

Manga, M., Rowland, J.C., 2009. Response of Alum Rock springs to the October 30, 2007 Alum Rock earthquake and implications for the origin of increased discharge after earthquakes. Geofluids 9, 237–250.

Manga, M., Wang, C.-Y., Shirzaei, M., 2016. Increased stream discharge after 3 September 2016 Mw 5.8 Pawnce. Oklahoma Earthquake. Geophysical Research Letters 43, 11588–11594.

Mantovani, E., Viti, M., Babbucci, D., Tamburelli, C., Vannucchi, A., Falciani, F., Cenni, N., 2014. Assetto tettonico e potenzialità sismogenetica dell'Appennino Tosco-Umbro-Marchigiano. Università di Siena, Siena, Italy.

Marchesini, E., 1946. Studio geologico del Monte Conero (Ancona). Giorn. Geol. 2 (18), 5–28.

Martinelli, G., 2020. Previous, current and future trends in research into earthquake precursors in geofluids. Geosciences 10 (5), 189.

Martinelli, G., Facca, G., Genzano, N., Gherardi, F., Lisi, M., Pierotti, L., Tramutoli, V., 2020. Earthquake-related signals in central Italy detected by hydrogeochemical and satellite techniques. Front. Earth Sci. 8, 584716.

Martinelli, G., Tamburello, G., 2020. Geological and geophysical factors constraining the occurrence of earthquake precursors in geofluids. Front. Earth Sci. 8, 596050.

Mattioli, A., 2014. Il bacino del fiume Aspio: assetto geostrutturale, geomorfologia e idrogeologia nell'analisi delle pericolosità idrogeologiche. Università Politecnica delle Marche. Ph.D. Thesis.

Mazzoli, S., Helman, M., 1994. Neogene patterns of relative plate motion for Africa-Europe: some implications for recent central Mediterranean tectonics. Geol. Rundsch. 83, 464–468.

Mazzoli, S., Machiavelli, C., Ascione, A., 2014. The 2013 Marche off-shore earthquakes: new insights into the active tectonic setting of the outer-northern Apennines. J. Geol. Soc. 171, 457–460.

Mazzoli, S., Pierantoni, P.P., Borraccini, F., Paltrinieri, W., Deiana, G., 2005. Geometry, segmentation pattern and displacement variations along a major Apennine thrust zone, central Italy. J. Struct. Geol. 27, 1940–1953.

Mazzoli, S., Santini, S., Macchiavelli, C., Ascione, A., 2015. Active tectonics of the outer Northern Apennines: Adriatic vs. Po Plain Seismicity. J. Geodynamics 84, 62–76.

Middelburg, J.J., van der Weijden, C.H., Woittiez, J.R., 1988. Chemical processes affecting the mobility of major, minor and trace elements during weathering of granitic rocks. Chem. Geol. 68 (3–4), 253–273.

Mussi, M., Nanni, T., Tazioli, A., Vivalda, P., 2017. The Mt. Conero limestone ridge: the contribution of stable isotopes to the identification of recharge areas of aquifers. Ital. J. Geosci. 136 (2), 186–187.

Nanni, T., 1980. Note illustrative sulla carta geologica dell'anconetano. Ed. Reg. Marche-Comune di Ancona, pp. 55.

Nanni, T., 1991. Cartografia geologico tecnica ai fini urbanistici del territorio del comune di Ancona alla scala 1:10.000. Regione Marche – Universtià degli Studi di Ancona (technical relation).

Nanni, T., Coltorti, M., Garziano, C. A., 1997. Carta geologica, idrogeologica e geomorfologica del bacino del fiume Musone. In: Il bacino del fiume Musone, Geologia, Geomorfologia e Idrogeologia, 15-47. Ass. Comuni di Osimo, Castelfidardo e Offagna. SELCA, Firenze.

Nanni, T., Vivalda, P., 1999. Le acque salate dell'Avanfossa marchigiana: origine, chimismo e caratteri strutturali delle zone di emergenza. Bollettino Della Società Geologica Italiana 118, 191–215.

Nanni, T., Vivalda, P., 2005. The aquifers of the Umbria-Marche Adriatic region: relationships between structural setting and groundwater chemistry. Boll. Soc. Geol. It. 124, 523–542.

Palme, H., O'Neill, H.S.T.C., 2014. Cosmochemical estimates of mantle composition. Elsevier, In The mantle and core, pp. 1–39.

Parkhurst, D.L., Appelo, C.A.J., 2013. Description of input and examples for PHREEQC version 3—a computer program for speciation, batch-reaction, one-dimensional transport, and inverse geochemical calculations. US Geological Survey Techniques and Methods 6 (A43), 497.

Patacca, E., Scandone, P., Bellatalla, M., Perilli, N., Santini, U., 1991. La zona di giunzione tra l'arco appenninico settentrionale e l'arco appenninico meridionale nell'Abruzzo e nel Molise. Studi Geologici Camerti, Special Volume, pp. 417–441.

Petitta, M., Mastrorillo, L., Preziosi, E., Banzato, F., Barberio, M.D., Billi, A., Cambi, C., De Luca, G., Di Carlo, G., Di Curzio, D., Di Salvo, C., Nanni, T., Palpacelli, S., Rusi, S., Saroli, M., Tallini, M., Tazioli, A., Valigi, D., Vivalda, P., Doglioni, C., 2018. Water-table and discharge changes associated with the 2016-2017 seismic sequence in Central Italy: hydrogeological data and a conceptual model for fractured carbonate aquifers. Hydrgeol. J. 26 (4), 1009–1026.

Pezzo, G., Billi, A., Carminati, E., De Gori, P., Devoti, R., Lucente, F.P., Palano, M., Petracchini, L., Serpelloni, E., Tavani, S., Chiarabba, C., 2023. Seismic source of identification of the 9 November 2022 Mw 5.5 offshore Adriatic Sea (Italy) earthquake from GNSS data and aftershock relocation. Sci. Rep. 13, 11474.

Pierantoni, P.P., Chicco, J., Costa, M., Invernizzi, C., 2019. Plio-Quaternary transpressive tectonics: a key factor in the structural evolution of the outer Apennine-Adriatic system. Italy. J. Geol. Soc. 176 (6), 1273–1283.

Reddy, D.V., Kumar, D., Rao, P.N., 2017. Long-term hydrochemical earthquake precursor studies at Konya-Warna reservoir site in Western India. J. Geol. Soc. India 90, 720–727.

Rovida, A., Locati, M., Camassi, R., Lolli, B., Gasperini, P., Antonucci, A., 2022. Italian Parametric Earthquake Catalogue (CPTI15), version 4.0. Istituto Nazionale Di Geofisica e Vulcanologia (INGV).

Sarti, M., Coltorti, M., 2014. Note illustrative della carta geologica d'Italia alla scala 1: 50.000. Foglio 293, Osimo. ISPRA-Roma.

Scisciani, V., 2009. Styles of positive inversion tectonics in the Central Apennines and in the Adriatic foreland: implications for the evolution of the Apennine chain. J. Struct. Geol. 31, 1276–1294.

Sil, S., Freymueller, J.T., 2006. Water level changes in Fairbanks, Alaska, due to the great Sumatra-Andaman earthquake. Earth Planets Space 651, 232–241.

Skelton, A., Andrén, M., Kristmannsdóttir, H., Stockmann, G., Mörth, C.-M., Sveinbjörnsdòttir, A., Jónsson, S., Sturkell, E., Guorúnardóttir, H.-R., Hjartarson, H., Siegmund, H., Kockum, I., 2014. Changes in groundwater chemistry before two consecutive earthquakes in Iceland. Nat. Geosci. 7, 752.

Skelton, A., Claesson, L., Wästeby, N., Andrén, M., Stockmann, G., Sturkell, E., Mörth, C.-M., Stefansson, A., Tollefsen, E., Siegmund, H., Keller, N., Kjartansdóttir, R., Hjartarson, H., Kockum, I., 2019. Hydrochemical changes before and after earthquakes based on long-term measurements of multiple parameters at two sites in Northern Iceland - a review. J. Geophys. Res. Solid Earth 124, 2702–2720.

Skelton, A., Sturkell, E., Mörth, C.-M., Stockmann, G., Jónsson, S., Stefansson, A., Liljedahl-Claesson, L., Wästeby, N., Andrén, M., Tollefsen, E., Robin, J.G., Keller, N., Geirsson, H., Hjartarson, H., Kockum, I., 2024. Towards a method for forecasting earthquakes in Iceland using changes in groundwater chemistry. Commun. Earth Environ. 5, 662.

Tazioli, A., Mattioli, A., Nanni, T., Vivalda, P., 2015. Natural hazard analysis in the Aspio equipped basin. "Engineering geology for society and territory; river basins, reservoir sedimentation and water resources", 3, 431-435.

Teloni, S., Valente, E., Ascione, A., Mazzoli, S., Pierantoni, P.P., Invernizzi, M.C., 2024. Morphological evidence of crustal-scale, active along-strike segmentation of the Umbria-Marche Apennines, Italy. Tectonophysics 891, 230527.

Thomas, D., 1988. Geochemical precursors to seismic activity. Pure Appl. Geophys. 126, 241–266.

Thorstenson, D.C., 1984. The concept of electron activity and its relation to redox potentials in aqueous geochemical systems: US Geol. Survey Open-File Rept 84 (072), 67.

Turco, E., Machiavelli, C., Mazzoli, S., Schettino, A., Pierantoni, P.P., 2021. Kinematics of deformable rocks: application to the opening of the Tyrrhenian basin and the formation of the Apennine chain. Geosciences 11 (4), 177.

Valigi, D., Fronzi, D., Cambi, C., Beddini, G., Cardellini, C., Checcucci, R., Mastrorillo, L., Mirabella, F., Tazioli, A., 2020. Earthquake-induced spring discharge modifications: The Pescara di Arquata spring reaction to the August–October 2016 Central Italy earthquakes. Water 12 (3), 767.

Vannoli, P., Basili, R., Valensise, G., 2004. New geomorphic evidence for anticlinal growth driven by blind-thrust faulting along the northern Marche coastal belt (central Italy). J. Seismol. 8, 297–312.

Vannoli, P., Vannucci, G., Bernardi, F., Palombo, B., Ferrari, G., 2015. The source of the 30 October 1930 Mw 5.8 Senigallia (Central Italy) earthquake: a convergent solution from instrumental, macroseismic and geological data. Bull. Seismol. Soc. Am. 105 (3), 1548–1561.

Wang, C.-Y., Manga, M., 2015. New streams and springs after the 2014 Mw 6.0 South Napa earthquake. Nat. Commun. 6, 7597.

Wang, C.-Y., Manga, M., 2021. Water and earthquakes. Springer Nature.

Yadav, S.K., Ramanathan, A.L., Kumar, M., Chidambaram, S., Gautam, Y.P., Tiwari, C., 2020. Assessment of arsenic and uranium co-occurrences in groundwater of central Gangetic Plain, Uttar Pradesh, India. Environ. Earth Sci. 79 (6), 154.

Zappa, G., Bersezio, R., Felletti, F., Giudici, M., 2006. Modeling heterogeneity of gravel-sand, braided stream, alluvial aquifers at the facies scale. J. Hydrol. 325 (1–4), 134–153.

Zinn, B.A., Konikow, L.F., 2007. Effects of intraborehole flow on groundwater age distribution. Hydrgeol. J. 15, 633–643.